Peer Review Status

This is a non-peer-reviewed preprint submitted to EarthArXiv.

This manuscript has been submitted to Environmental Research Communications (IOP Publishing; manuscript reference ERC-105996) for peer review and is currently under revision.

Title

Extreme Precipitation Indices Trends and Patterns in the Philippines

Authors

Arnold R. Salvacion1,2,*, Allen L. Nazareno3, Destiny S. Lutero3

[1] Curtin Biometry and Agricultural Data Analytics, Curtin University, Perth 6102, Australia

[2] Department of Community and Environmental Resource Planning, University of the Philippines Los Baños

[3] Institute of Mathematical Sciences, University of the Philippines Los Baños

* Corresponding author

Email addresses:

Arnold R. Salvacion: arnold.salvacion@curtin.edu.au

Allen L. Nazareno: alnazareno@up.edu.ph

Destiny S. Lutero: dslutero@up.edu.ph

Extreme Precipitation Indices Trends and Patterns in the Philippines

Arnold R. Salvacion[1,2], Allen L. Nazareno[3], Destiny S. Lutero[3]

[1] Curtin Biometry and Agricultural Data Analytics, Curtin University, Perth 6102, Australia

[2] Department of Community and Environmental Resource Planning, University of the Philippines Los Baños

[3] Institute of Mathematical Sciences, University of the Philippines Los Baños

Email: arnold.salvacion@curtin.edu.au

Abstract

The Philippines experiences approximately 86% of its recorded disaster events from extreme precipitation, yet national-scale trend studies remain constrained by sparse station networks and narrow index coverage. This study mapped the spatial patterns and long-term trends of 12 extreme precipitation indices across the Philippine archipelago using 45 years of daily gridded precipitation data from the Climate Hazards Group InfraRed Precipitation with Stations dataset over the period 1981 to 2025. Trend magnitude and direction were estimated at each grid cell using the Theil-Sen slope estimator and assessed for statistical significance using the Mann-Kendall test; spatial clustering of trends was examined using the Local Indicator of Spatial Association. Field-significance testing (Monte Carlo permutation) and a Hamed-Rao (1998) autocorrelation correction were subsequently applied to determine which spatial trend patterns are distinguishable from spatially correlated noise. Significant increasing trends in total annual precipitation covered 71.9% of land grid cells (Hamed-Rao-corrected; 60.5% raw) with a median Sen's slope of 17.6 mm yr^{-1}, concentrated predominantly in Mindanao and the Visayas, with central Luzon and southern Luzon (Bicol) as secondary contributors, and this pattern was field-significant ($p = 0.004$). Heavy precipitation frequency showed the most spatially extensive and most robust signal, with significant increasing trends in heavy rainfall days covering up to 73.1% of land grid cells (R10; field-significant, $p = 0.010$). Re-analysis found mean daily rainfall intensity on wet days (SDII) to be predominantly increasing, not decreasing as initially reported, across 25.6% of land grid cells, though this pattern did not reach field significance ($p = 0.058$) and is therefore suggestive rather than conclusive. Rainfall days are consequently becoming more frequent across much of the country with high statistical confidence, while evidence for a corresponding change in per-event intensity remains inconclusive, a more conservative conclusion than a straightforward frequency-versus-intensity dichotomy. The contrasting trend directions between 3-day and 5-day maximum accumulations are suggestive of, but do not on their own demonstrate, a lengthening of sustained rainfall episodes, since the 5-day signal did not reach field significance ($p = 0.115$). Spatial clustering analysis, computed on the complete spatial field of Sen's slopes, identified hotspot clusters concentrated on the typhoon-exposed eastern seaboard, including western Mindanao and the Zamboanga Peninsula for the two most robust frequency indices (R10, R20), and a coldspot cluster concentrated in northern Luzon; these results inform flood risk management and agricultural water planning across the exposure-sensitive sub-regions identified.

Keywords: CHIRPS; Mann-Kendall trend test; spatial analysis; GIS

1. INTRODUCTION

Anthropogenic climate change is intensifying the global water cycle through a well-established thermodynamic mechanism: for every 1°C of atmospheric warming, the Clausius–Clapeyron relationship dictates that air can hold approximately 7% more water vapour, implying a 14% increase in atmospheric moisture content at 2°C of global warming (Adam, 2023). This moisture loading drives simultaneous increases in atmospheric evaporative demand (AED) and in the moisture available for precipitation, thereby amplifying both drought and flood extremes across the hydrological cycle (Mullens et al., 2013; Trenberth, 2011). Consistent with these thermodynamic expectations, Ajjur and Al-Ghamdi (2021) estimated increases in potential evapotranspiration (PET) of 0.37–0.51 mm yr^{-1} in the Middle East and North Africa under SSP2-4.5, while Vahmani et al. (2022) reported a 1% increase in evapotranspiration per 1°C warming in California. These changes in the hydrological cycle have direct consequences for water resource systems and hydrological processes globally (Lima et al., 2015; Rana et al., 2014; Tabari, 2020), and delineating where precipitation extremes are intensifying is therefore essential for targeted climate risk mitigation.

The sectoral consequences of changing extreme precipitation extend well beyond water resources. In agriculture, extreme climatic events explain 50–60% of yield losses in maize based on a six-year field experiment in China (Deng et al., 2026), while negative trends in annual rainfall and consecutive dry days have reduced rice cultivation in parts of Upper Ganga, India (Das et al., 2024). In contrast, Santos et al. (2022) reported a positive correlation between extreme precipitation indices and rainfed crop yield in Nebraska, USA, underscoring the context-dependence of agricultural impacts. For terrestrial ecosystems and water resources, Ren et al. (2025) estimated that water yield and erosion rates in Sichuan, China increase proportionally with intensifying extreme precipitation trends, and Zhu et al. (2024) reported that 60–90% of nitrate leaching in an agriculturally intensive region in China is attributable to extreme precipitation events. In terms of public health, extreme precipitation has been associated with ischaemic stroke hospitalisation in Anhui Province, China (Tang et al., 2020), with schizophrenia hospitalisations elsewhere in the country (Liu et al., 2022), and with diarrheal infection in Taiwan (Andhikaputra et al., 2023). These findings underscore that understanding the spatial patterns and long-term trends of extreme rainfall is indispensable for assessing and mitigating negative impacts across food, water, and health systems.

Extreme precipitation indices (EPIs) are standardised metrics developed to quantify the amount, intensity, frequency, and persistence of rainfall distributions across spatial domains. These indices include measures of total precipitation, the number of wet and dry days, and consecutive wet and dry day sequences (Rodríguez-González and Cerezo-Mota, 2025; WCRP, 2025). Table 1 summarises the 12 indices applied in this study, along with their descriptions, abbreviations, and units.

Table 1. *Selected daily precipitation-based extreme precipitation indices used in this study*

Index	Description	Abbreviation	Unit
Annual total precipitation	Cumulative annual precipitation from daily data	PRCPTOT	mm
Very wet days	Annual total precipitation from wet days (RR ≥ 1 mm) exceeding the 95th percentile of the 1981–2025 wet-day distribution	R95p	mm
Extremely wet days	Annual total precipitation from wet days (RR ≥ 1 mm) exceeding the 99th percentile of the 1981–2025 wet-day distribution	R99p	mm
Maximum 1 day precipitation	Highest amount of precipitation in 1 day	RX1day	mm
Maximum 3-day precipitation	Highest amount of precipitation for 3 consecutive days	RX3day	mm
Maximum 5-day precipitation	Highest amount of precipitation 5 consecutive days	RX5day	mm
Simple daily intensity index	Average precipitation per wet days	SDII	mm/day
Consecutive wet days	Maximum number of days with precipitation ≥ 1 mm	CWD	days
Consecutive dry days	Maximum number of days with precipitation < 1 mm	CDD	days
Heavy precipitation days	Number of days with precipitation ≥ 10 mm	R10	days
Very heavy precipitation days	Number of days with precipitation ≥ 20 mm	R20	days
Extremely heavy precipitation days	Number of days with precipitation ≥ 30 mm	R30	days

Several studies have applied EPIs to characterise extreme precipitation trends at regional and global scales, yielding predominantly increasing signals in typhoon-exposed and monsoon-dominated regions. In northern Pakistan, EPIs derived from historical and projected climate data revealed increasing extreme precipitation trends (Saddique et al., 2020), consistent with findings from the Yucatan Peninsula of Mexico over 1980–2010 (Rodríguez-González and Cerezo-Mota, 2025). In China, multiple studies reported increasing extreme precipitation trends under both historical records and future projections under RCP 8.5 (Gan et al., 2022; Li et al., 2021; Wang et al., 2023), and ensemble projections for Thailand estimated increasing extremes across the country (Rojpratak and Supharatid, 2022). In contrast, downward EPI trends were reported from weather station data in Nigeria (1983–2017; Ogolo and Matthew, 2022), while trends in Bangladesh were found to be localised rather than regionally coherent (Abdullah et al., 2022). At the global scale, analyses of reanalysis precipitation data generally report an overall increasing tendency (Dunn et al., 2022; Li et al., 2024), and studies in Iran document spatially contrasting trends reflecting regional topographic and climatic heterogeneity (Fattahi et al., 2025).

The Philippines ranks among the world's most climate-vulnerable nations, with extreme precipitation events constituting the dominant natural hazard. From 2000 to 2025, approximately 86% of all recorded disaster events in the country were attributable to extreme precipitation (Delforge et al., 2025; Olaguera et al., 2022), with storm events and associated flooding accounting for 94% of events over this period (Delforge et al., 2025). More than 1 million Filipinos are exposed to flash floods annually due to heavy precipitation from tropical cyclones (Rivera and Dela Vega, 2025). Typhoon Fengshen (2008) delivered 345 mm of rainfall in 24 hours across Panay Island, affecting more than 1.7 million individuals at an estimated cost of USD 252 million (Yumul et al., 2012), while Typhoon Ketsana (locally known as Ondoy; 2009) dropped 448.5 mm in 12 hours over Metro Manila, affecting more than 1 million Filipinos at an estimated cost of USD 43.5 billion (Abon et al., 2011). Spatially comprehensive monitoring of extreme precipitation trends across the Philippines is therefore a national priority.

Despite this exposure, existing Philippine precipitation trend studies are constrained by limited spatial coverage and narrow index sets. Cruz et al. (2013) examined Southwest Monsoon rainfall trends from 1961 to 2010 using only 9 stations along the western seaboard, finding significant decreasing trends at 6 stations. Cinco et al. (2014) detected trends in only two EPIs from 34 synoptic stations over 1951–2010, with just 4 stations showing weak increasing trends.

Villafuerte et al. (2014) extended this dataset to 7 EPIs across seasonal quarters but still found contrasting and spatially incoherent signals. These gaps are largely attributable to the limited public availability of high-resolution weather station records in the Philippines (Salvacion et al., 2018), which has historically constrained national-scale EPI assessments.

The Climate Hazards Group InfraRed Precipitation with Stations (CHIRPS) dataset provides a high-resolution (0.05° × 0.05°) gridded daily precipitation record extending from 1981 to the present, combining satellite-derived estimates with station data (Funk et al., 2015). CHIRPS has been applied in more than 100 published validation studies globally, with the majority concentrated in Asia (n = 55) and Africa (n = 48), and generally demonstrates strong monthly-scale performance across Asian domains ($R^2 > 0.8$; Du et al., 2024). In the Philippines, Alejo and Alejandro (2021) validated CHIRPS against 68 rainfall stations and found that performance is modulated by climate type, with adequate reproduction of monthly rainfall amounts in approximately half of the stations tested. Peralta et al. (2020) further evaluated CHIRPS against daily data from 49 stations and concluded that it captures seasonal rainfall peaks well and outperforms other gridded datasets on standard error metrics, supporting its suitability for calculating rainfall-based climate indices at national scale.

The goal of this study is to determine the spatial patterns and long-term trends of extreme precipitation indices across the Philippines using CHIRPS daily precipitation data from 1981 to 2025. Specifically, this study aims to: 1) document the spatial distribution of mean annual values for 12 EPIs across the Philippine archipelago; 2) identify grid cells with statistically significant increasing or decreasing EPI trends using the Mann-Kendall test and quantify trend magnitude using Theil-Sen slope estimation with 95% confidence intervals; and 3) delineate significant spatial clusters of EPI trends using Local Indicator of Spatial Association (LISA) analysis to identify hotspot and coldspot zones. Knowledge of the spatial patterns and trends of extreme precipitation can support location-specific, science-based approaches to minimising damage and losses from climate-driven hydrological extremes.

2. METHODOLOGY

2.1 Study Area

The Philippines (Fig. 1) is characterised by exceptional topographic and climatic complexity for an archipelagic nation — comprising more than 7,600 islands positioned between Taiwan and Borneo, approximately 800 km from the Asian mainland (Boquet, 2017). The islands are grouped into three major island clusters: Luzon in the north, the Visayas in the centre, and Mindanao in the south (Fig. 2a). This geographic configuration, combined with north-to-south mountain ranges that bisect the major islands, produces pronounced rainfall gradients under the Philippine Corona System (Ibarra et al., 2021; Tolentino et al., 2016), which classifies the country into four climate types (Fig. 2b). Type I climate, found along the western seaboard, exhibits well-defined wet (May–October) and dry (November–April) seasons driven by the summer monsoon. Type II climate along the eastern seaboard lacks a distinct dry season, receiving peak rainfall from November to February due to direct exposure to the northeast monsoon and passing typhoons. Type III climate, characterising inland areas, receives lower annual rainfall with a brief dry period from December to May. Type IV climate in the southeastern inland regions is marked by relatively low and seasonally uniform rainfall throughout the year.

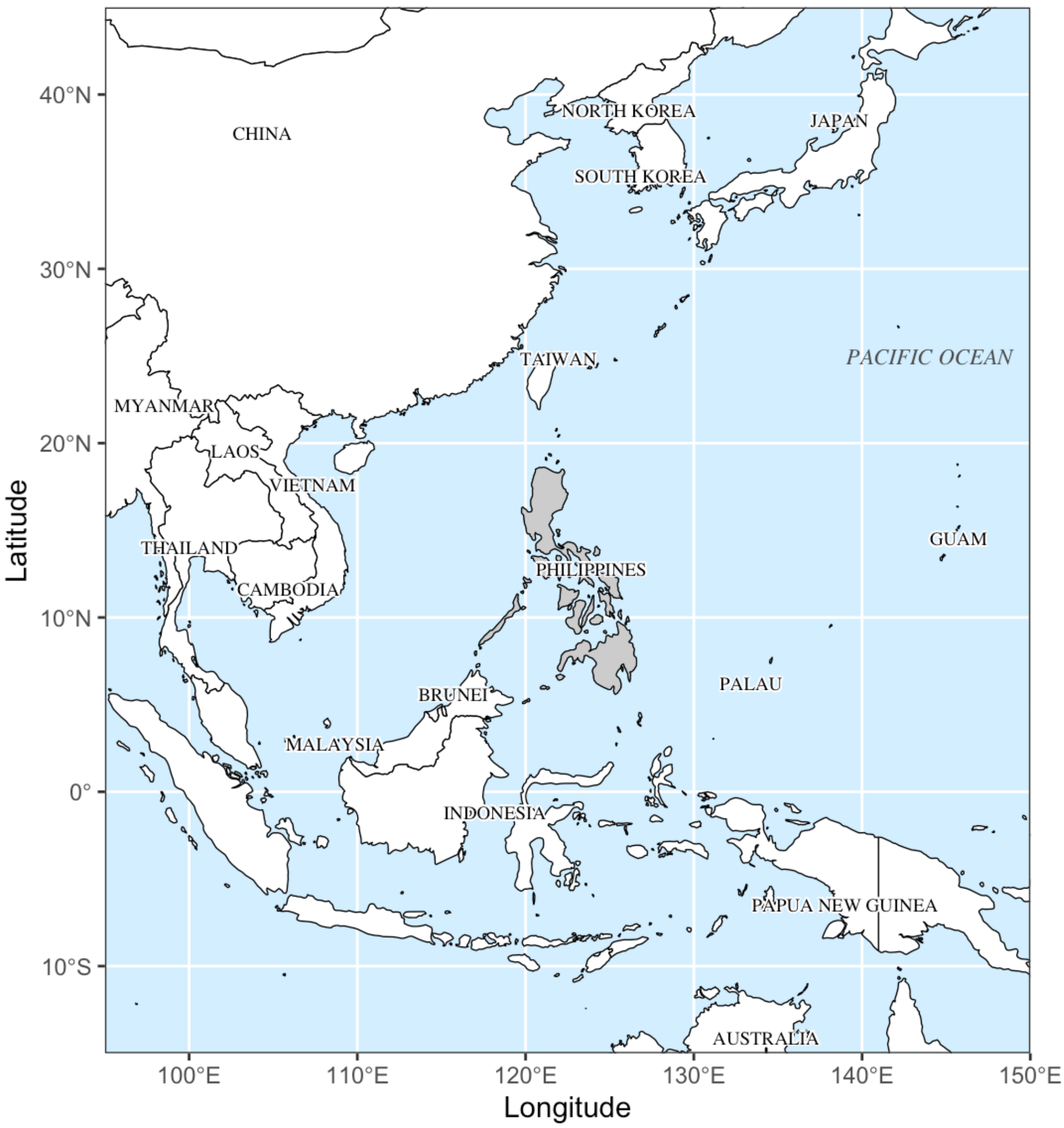

Figure 1. *Location map of the Philippines within the Asia-Pacific region, highlighting its geographic position relative to neighbouring countries and territories. The Philippines, shown in grey, is an archipelagic nation situated between approximately 5°N and 21°N latitude and 116°E and 127°E longitude. Country boundary data were obtained from the Natural Earth database and accessed using the rnaturalearth and rnaturalearthdata packages in R (Massicotte and South, 2026).*

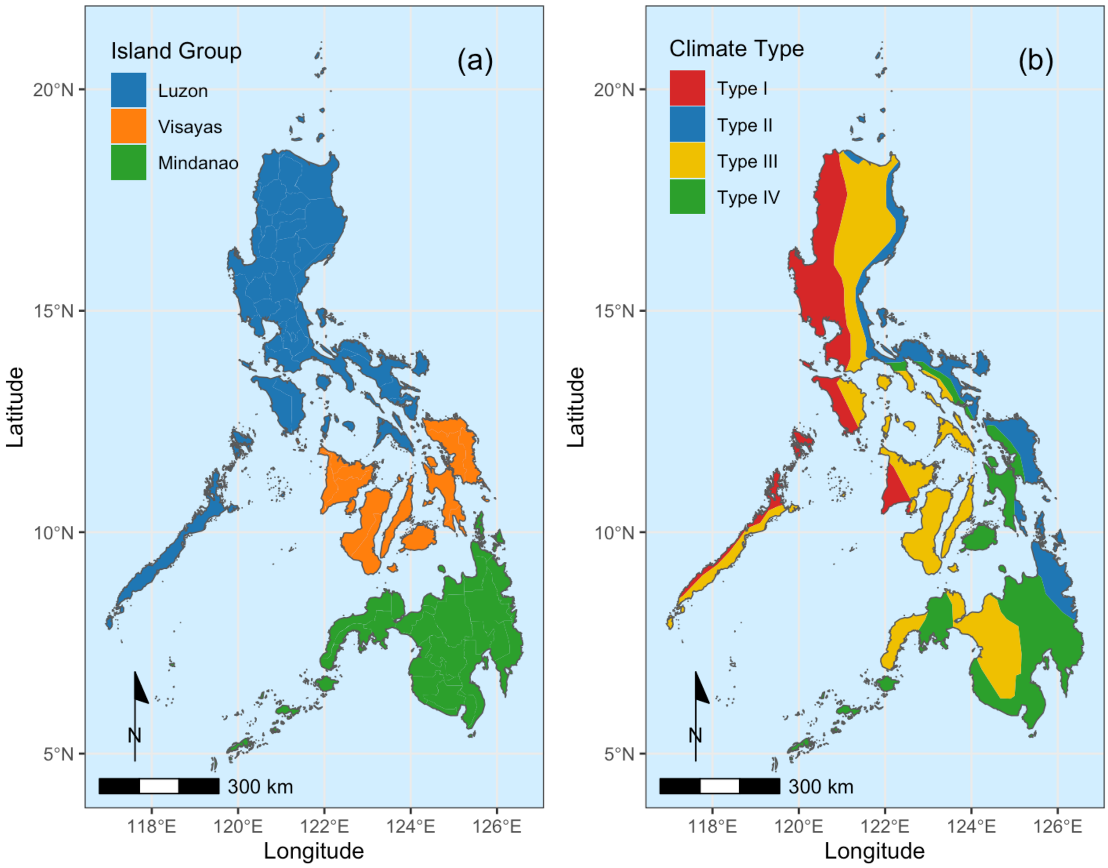

Figure 2. *Maps showing (a) major island group in the Philippines, and (b) the Philippines Corona System. The major island group of the Philippines were Luzon, Visayas, and Mindanao. The Philippine Corona System classified the country into four climate types (Types I–IV), distinguished primarily by the timing and distribution of wet and dry seasons; see Section 2.1 for a full description of each type. Note: Climate type map of the Philippines was digitized and redrawn from an existing online image published by the Philippine Atmospheric, Geophysical and Astronomical Services Administration (PAGASA).*

2.2 Data Processing and Analysis

Daily precipitation data from 1981 to 2025 were extracted for the Philippines from the CHIRPS gridded dataset at 0.05° × 0.05° resolution. Annual values for each of the 12 extreme precipitation indices (Table 1) were calculated per grid cell using the climatrends package (Sousa et al., 2023) in R (R Core Team, 2025). The magnitude and direction of long-term change were estimated for each index at each grid point using the Theil-Sen slope estimator (Theil, 1992; Nguyen et al., 2022) and assessed for statistical significance using the Mann-Kendall trend test (Hamed, 2008; Nguyen et al., 2022) via the raster.kendall function in the spatialEco package (Evans and Murphy, 2025). Both procedures are robust non-parametric methods well suited to trend detection in hydrological time series subject to non-normality and outliers (Abdullah et al., 2022; Techamahasaranont et al., 2017). The 95% confidence intervals for Sen's slope estimates were derived from the Mann-Kendall variance framework using the zyp package (Bronaugh and Schoeneberg, 2023) in R. Mean annual values of each index were calculated across the full study period to characterise the climatological spatial distribution. Spatial autocorrelation in EPI trend slopes was subsequently examined using the Local Indicator of Spatial Association (LISA; Anselin, 1995) to identify statistically significant hotspot (High-High) and coldspot (Low-Low) clusters, as well as spatial transition zones (High-Low and Low-High).

For reproducibility, CHIRPS v2.0 daily precipitation data were obtained from the Climate Hazards Center, University of California, Santa Barbara (https://data.chc.ucsb.edu/), consistent with the dataset version described by Funk et al. (2015). A land grid cell was defined as any $0.05° \times 0.05°$ cell with a non-missing precipitation value in the native CHIRPS product; ocean and open-water cells are stored as missing (NaN) in the CHIRPS grid itself and were excluded on this basis, without requiring a separate administrative land mask. This yielded 9,839 valid land grid cells across the Philippines out of 63,497 total grid cells within the study extent (116.95–126.6°E, 4.6–21.05°N). No interpolation or gap-filling was applied to missing daily values; a year with incomplete daily coverage at a given cell is reflected as a missing value in that cell's annual index for that year, and grid cells with fewer than 10 complete annual values over 1981–2025 were excluded from trend estimation. Analyses were conducted in R version 4.5.2 (R Core Team, 2025) using the packages cited throughout this section; exact package version numbers are available on request.

For the percentile-based indices (R95p, R99p), the wet-day threshold followed the standard ETCCDI convention ($RR \geq 1$ mm; Zhang et al., 2011), consistent with the implementation approach of Rodríguez-González and Cerezo-Mota (2025). Percentile thresholds were calculated from the full 1981–2025 record rather than a separate, independent reference period; CHIRPS coverage begins in 1981, so no earlier independent baseline was available. This setting is reported here for reproducibility, consistent with the climatrends package's implementation of these indices (Sousa et al., 2023).

LISA cluster classification was based on local Moran's I computed on standardised (z-scored) Sen's slope values for the complete spatial field of land grid cells, rather than a subset pre-filtered to Mann-Kendall-significant cells (Section 3.1.0). Spatial weights were constructed using $k = 8$ nearest neighbours identified by great-circle distance, with row-standardised weights (each neighbour weighted 1/k); k-nearest-neighbour weights were used rather than polygon contiguity because the archipelagic, non-contiguous structure of Philippine land grid cells would otherwise leave isolated island cells without neighbours. Local significance was assessed via a conditional permutation test (999 permutations per cell) at $\alpha = 0.05$, with permutation p-values corrected for multiple local testing using the Benjamini-Hochberg false discovery rate procedure; a grid cell was classified as High-High, Low-Low, High-Low, or Low-High only where both the local sign pattern and the FDR-corrected local p-value met this threshold, and as not significant otherwise.

3. RESULTS

3.1 Spatial Pattern and Trends in Extreme Precipitation Indices

Nine of the 12 EPIs examined exhibited net increasing trends across significant grid cells over the period 1981–2025, with the largest median Sen's slopes recorded for the precipitation amount indices (PRCPTOT: 17.6 mm yr^{-1}; R95p: 6.0 mm yr^{-1}) and the most spatially extensive significant trends recorded for the heavy precipitation frequency indices (R10: 73.1%, R20: 61.2% of land grid cells, Hamed-Rao-corrected). Table 2 summarises the direction, spatial extent, and magnitude (median Sen's slope with 95% confidence interval) of statistically significant trends across all 12 EPIs, and the following subsections describe the spatial distribution and trend structure of each index group in detail.

Statistical robustness of grid-cell trends. Grid-cell Mann-Kendall trend tests reported above and in Table 2 incorporate a field-significance test accounting for spatial autocorrelation among grid cells, and a temporal-autocorrelation correction following Hamed and Rao (1998). Lag-1 autocorrelation was present to varying degrees across the 12 indices, ranging from negligible for RX3day (mean $r1 = 0.003$) to substantial for SDII (mean $r1 = 0.280$) and PRCPTOT (mean $r1 = 0.219$). Applying the Hamed-Rao variance correction produced a numerically unstable result (a negative effective-sample-size ratio) for a small fraction of cells per index (0.1-3.1%); these cells were conservatively treated as non-significant.

Field significance was tested via a Monte Carlo permutation procedure (999 permutations) that preserves the spatial correlation structure of the CHIRPS grid while destroying any temporal trend, determining whether the areal extent of significant cells for each index exceeds what spatial autocorrelation alone would produce by chance. PRCPTOT, R10, R20, R30, and RX3day were field-significant at the 5% level (p = 0.004-0.044), indicating that the spatial pattern of significant trends for these indices is unlikely to be a multiple-testing artefact. RX1day, RX5day, SDII, CDD, R95p, and R99p did not reach field significance (p = 0.054-0.115), and CWD showed no distinguishable areal signal beyond chance (p = 0.409). These results, and the autocorrelation-corrected significant fractions for all 12 indices, are used throughout the remainder of Section 3 and Section 4 to distinguish statistically robust spatial patterns from patterns that cannot be distinguished from the effect of spatial autocorrelation.

Table 2. *Field-significance and autocorrelation-corrected trend summary for all 12 extreme precipitation indices across the Philippines, 1981–2025.*

Index	Raw % Inc.	Raw % Dec.	AC-corr. % Inc.	AC-corr. % Dec.	Field-sig. p	Robust?
PRCPTOT	60.5	0.0	71.9	0.0	0.004	Yes
R10	63.0	0.0	73.1	0.0	0.010	Yes
R20	56.2	0.0	61.2	0.0	0.007	Yes
R30	40.4	0.4	42.5	0.4	0.010	Yes
RX3day	6.4	6.0	8.9	7.2	0.044	Yes (marginal)
R95p	19.0	1.2	20.4	1.4	0.054	Borderline
RX1day	6.0	4.4	8.0	5.4	0.054	Borderline
SDII	31.9	0.2	25.6	0.3	0.058	Borderline (see note)
R99p	9.3	3.5	11.0	4.1	0.062	No
CDD	0.2	8.8	0.7	17.3	0.093	No
RX5day	6.5	3.8	8.6	4.8	0.115	No
CWD	5.0	0.3	6.9	0.5	0.409	No

Raw % Inc./Dec. are the percentage of land grid cells with a statistically significant (alpha = 0.05) increasing or decreasing Mann-Kendall trend under the original, uncorrected per-cell test. AC-corr. % Inc./Dec. apply the Hamed-Rao (1998) temporal-autocorrelation correction, treating numerically unstable corrections conservatively as non-significant. Field-sig. p is the Monte Carlo field-significance p-value (999 permutations), testing whether the areal extent of significant cells exceeds what spatial autocorrelation alone would produce by chance; indices with $p < 0.05$ are marked “Yes” in the Robust? column. Median Sen's slope and 95% CI values for the corrected significant-cell sets are pending recomputation and are not yet reproduced here.

3.1.1 Total Annual Precipitation (PRCPTOT)

Orographic control of the north-to-south mountain ranges that bisect Luzon and Mindanao drives a pronounced east-to-west rainfall gradient in mean annual PRCPTOT, with values exceeding 3,500 mm along the eastern coastal zones and interior mountain ranges of both island groups and falling below 1,000 mm across the western lowlands of Luzon, the Cagayan Valley floor, and the leeward coastal areas of the central Visayas and western Mindanao (Fig. 3a). This spatial structure reflects the dominant influence of orographic enhancement on windward slopes and rain shadow suppression on leeward lowlands.

Statistically significant PRCPTOT trends were spatially concentrated in the typhoon-exposed zones of the eastern seaboard, covering 60.5% of total land grid cells (71.9% after a Hamed-Rao autocorrelation correction; field-significance $p = 0.004$), predominantly across Mindanao (33.1% of significant cells) and the Visayas (24.4%), with central Luzon (14.2%) and southern Luzon/Bicol (13.9%) as secondary contributors (Fig. 3c; Table 2). The median Sen's slope across significant grid cells was 17.6 mm yr^{-1} (95% CI: 3.1–30.3 mm yr^{-1}), a magnitude consistent with warming-driven intensification of typhoon-associated rainfall in the western North Pacific, where rising sea surface temperatures increase available moisture along typhoon tracks in accordance with Clausius–Clapeyron scaling (Trenberth, 2011). Among the core significant zones, the narrowest CI widths were concentrated in Mindanao (mean 29.8 mm yr^{-1}) and the Visayas (30.5 mm yr^{-1}), reflecting relatively high temporal consistency of the trend signal in these typhoon-exposed zones; CI widths were widest in central Luzon (mean 32.5 mm yr^{-1}) (Fig. 3d), where the smaller, more scattered significant-cell footprint corresponds to greater interannual variability and reduced slope precision. The non-significance of 67.2% of grid cells across Palawan, the Zamboanga Peninsula, and much of Mindanao reflects the leeward positioning and reduced typhoon exposure of these sub-regions rather than an absence of directional change (Fig. 3b).

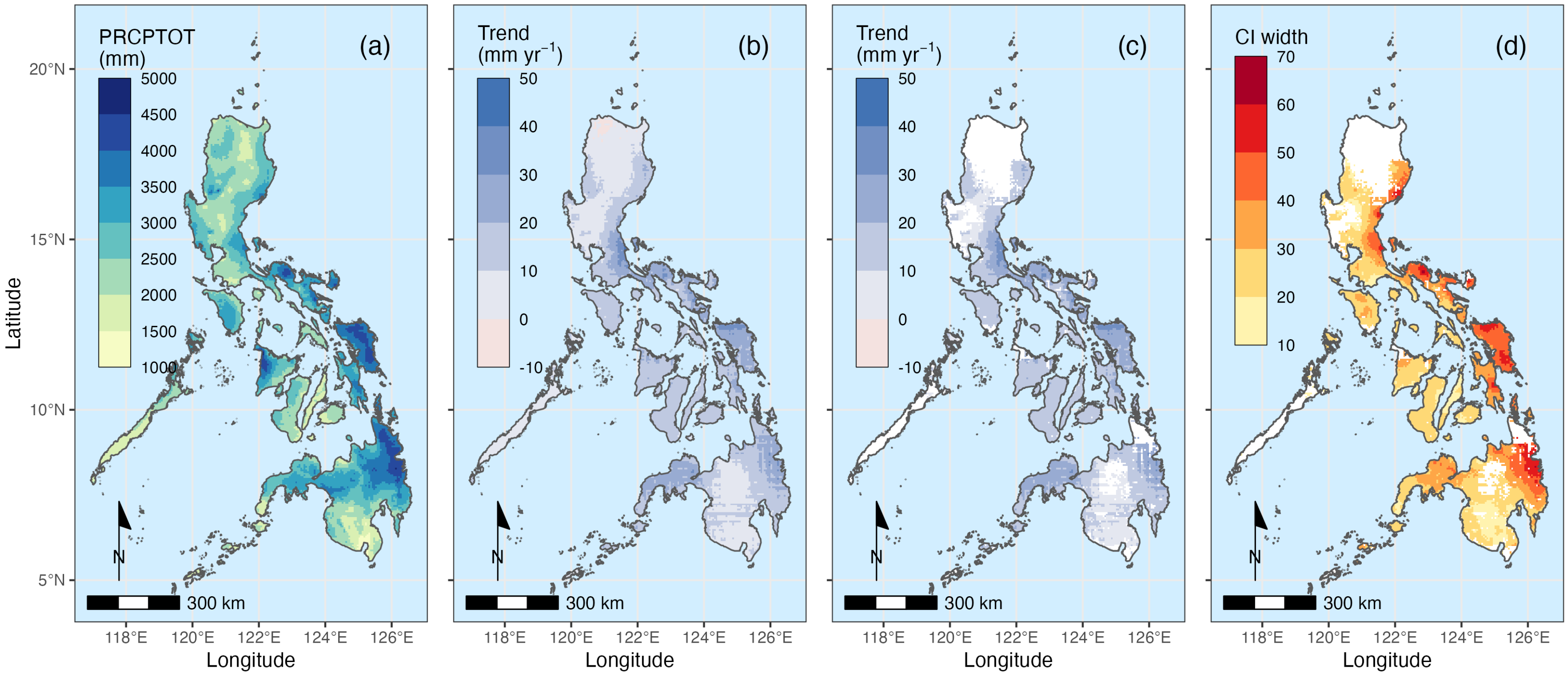

Figure 3. *Spatial distribution of mean annual total precipitation (PRCPTOT) and its long-term trends across the Philippines derived from Climate Hazards Group InfraRed Precipitation with Stations (CHIRPS) gridded rainfall data over the period 1981–2025. Panel (a) presents the mean annual PRCPTOT (mm), with higher values indicating wetter conditions. Panel (b) presents the Sen's slope estimate (mm yr^{-1}) for each grid cell, with positive values indicating increasing trends and negative values indicating decreasing trends over the study period; blue tones denote increasing trends and red tones denote decreasing trends as indicated by the diverging color scale. Panel (c) shows only those grid cells with statistically significant trends at α = 0.05 based on the Mann-Kendall trend test, with non-significant grid cells shown in white; color conventions follow panel (b). Panel (d) shows the 95% confidence interval width (mm) of the Sen's slope estimate for each statistically significant grid cell, with darker red tones indicating wider confidence intervals (lower precision in trend magnitude estimation) and lighter yellow tones indicating narrower confidence intervals (higher precision); non-significant grid cells are shown in white*

3.1.2 Wet Days (R99p and R95p)

Rainfall from the upper tail of the precipitation distribution is strongly concentrated on the typhoon-exposed eastern seaboard and mountainous interiors of Luzon and Mindanao: mean R99p values ranged from among the lowest in the dataset in the driest western areas to exceeding 800 mm along the eastern coast of Luzon and portions of eastern Mindanao, while R95p ranged from below 500 mm in the western lowlands to exceeding 2,000 mm in the most rainfall-exposed eastern zones (Fig. 4a and e).

Significant increasing trends in R99p were confined to a small cluster along the eastern coast of central Luzon and an isolated area in northeastern Luzon, with a median Sen's slope of 2.2 mm yr^{-1} (95% CI: 0.3–3.9 mm yr^{-1}), while broadly negative trends of approximately −2 to −4 mm yr^{-1} prevailed across northern Luzon, much of the Visayas, and large portions of Mindanao (Fig. 4b and c; Table 2). The 95% CI width for significant R99p grid cells ranged up to 14 mm (Fig. 4d), with the widest values in the isolated northeastern Luzon cluster, reflecting lower temporal signal consistency than along the core eastern coastal corridor. R95p showed a broadly comparable trend pattern at a substantially larger magnitude, with positive trends of up to 20 mm yr^{-1} along the eastern coast of Luzon and negative trends of approximately −5 to −7 mm yr^{-1} across northern Luzon, western Mindanao, and Palawan (Fig. 4f). Statistically significant increasing trends covered 20.4% of land grid cells (Hamed-Rao-corrected; 19.0% raw) with a median slope of 6.0 mm yr^{-1} (95% CI: 0.7–11.1 mm yr^{-1}), and a minor area of significant decreasing trends (1.4%) was identified in southeastern Mindanao (Fig. 4g; Table 2); this areal pattern did not reach field significance ($p = 0.054$) and is therefore suggestive rather than conclusive. R99p showed a comparable, also borderline pattern (11.0% increasing, 4.1% decreasing; $p = 0.062$). The 95% CI width for significant R95p grid cells reached up to 35 mm (Fig. 4h), more than double the maximum recorded for R99p, reflecting the greater sensitivity of the 95th-percentile threshold accumulation to interannual variability in mid-range rainfall magnitude.

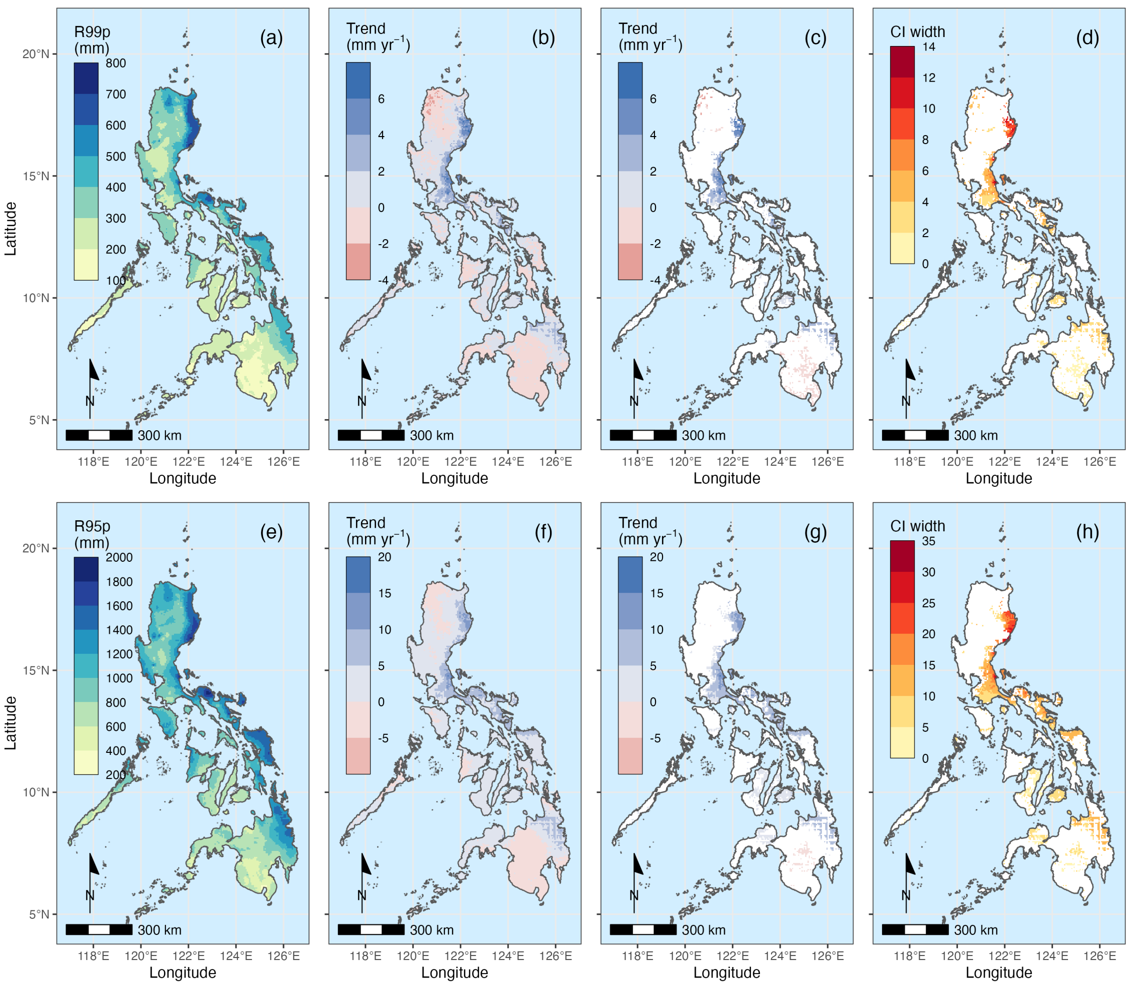

Figure 4. *Spatial distribution of mean annual extremely wet day (R99p) and very wet day (R95p) precipitation indices and their long-term trends across the Philippines derived from CHIRPS gridded rainfall data over the period 1981–2025. The upper row presents R99p: panel (a) shows the mean annual R99p (mm); panel (b) shows the Sen's slope estimate (mm yr⁻¹) for each grid cell, with blue tones denoting increasing trends and red tones denoting decreasing trends as indicated by the diverging color scale; panel (c) shows only those grid cells with statistically significant trends at α = 0.05 based on the Mann-Kendall trend test, with non-significant grid cells shown in white; and panel (d) shows the 95% confidence interval width (mm) of the Sen's slope estimate for each statistically significant grid cell, with darker red tones indicating wider confidence intervals (lower precision) and lighter yellow tones indicating narrower confidence intervals (higher precision), and non-significant grid cells shown in white. The lower row presents the corresponding maps for R95p, following the same layout: panel (e) shows mean annual R95p (mm); panel (f) shows the Sen's slope estimate; panel (g) shows statistically significant trends; and panel (h) shows the 95% confidence interval width (mm). Note that the CI width color scales differ between rows, reflecting the larger magnitude of R95p trend uncertainty relative to R99p. Non-significant grid cells are shown in white in panels (c), (d), (g), and (h).*

3.1.3 Short Duration Precipitation (RX1day, RX3day, and RX5day)

Short-duration maximum precipitation is dominated by the same orographic and typhoon-track controls as PRCPTOT: mean RX1day values ranged from among the lowest in the dataset in the western lowlands to exceeding 400 mm along the eastern coast of Luzon, while RX3day and RX5day reached peak values exceeding 600 mm in the most rainfall-exposed eastern zones of Luzon and northeastern Mindanao (Fig. 5a, e, and i).

Significant increasing trends in RX1day were confined to a narrow corridor along the eastern coast of central Luzon, with a median Sen's slope of 0.7 mm yr^{-1} (95% CI: 0–1.2 mm yr^{-1}) covering 8.0% of land grid cells (Hamed-Rao-corrected; 6.0% raw), while decreasing trends covered a comparable area (5.4%) in isolated portions of southeastern Mindanao (Fig. 5c; Table 2); this pattern did not reach field significance ($p = 0.054$). RX3day showed a significant decreasing trend (median slope: −0.5 mm yr^{-1}; 95% CI: −1 to −0.02 mm yr^{-1}) covering 8.9% of land grid cells (Hamed-Rao-corrected; 6.4% raw; field-significant, $p = 0.044$), while RX5day showed a significant increasing trend (median slope: 1.4 mm yr^{-1}; 95% CI: 0.1–2.7 mm yr^{-1}) covering 8.6% of land grid cells (not field-significant, $p = 0.115$). Because RX5day does not reach field significance, this contrast should be regarded as suggestive of, rather than demonstrating, a shift toward longer-duration sustained rainfall episodes, and event-based duration analysis would be required to confirm it. The 95% CI width for significant RX1day, RX3day, and RX5day grid cells ranged up to 6, 7, and 7 mm, respectively, with widths narrowest at the core of the eastern central Luzon corridor and widest at the spatial margins of significance (Fig. 5d, h, and l).

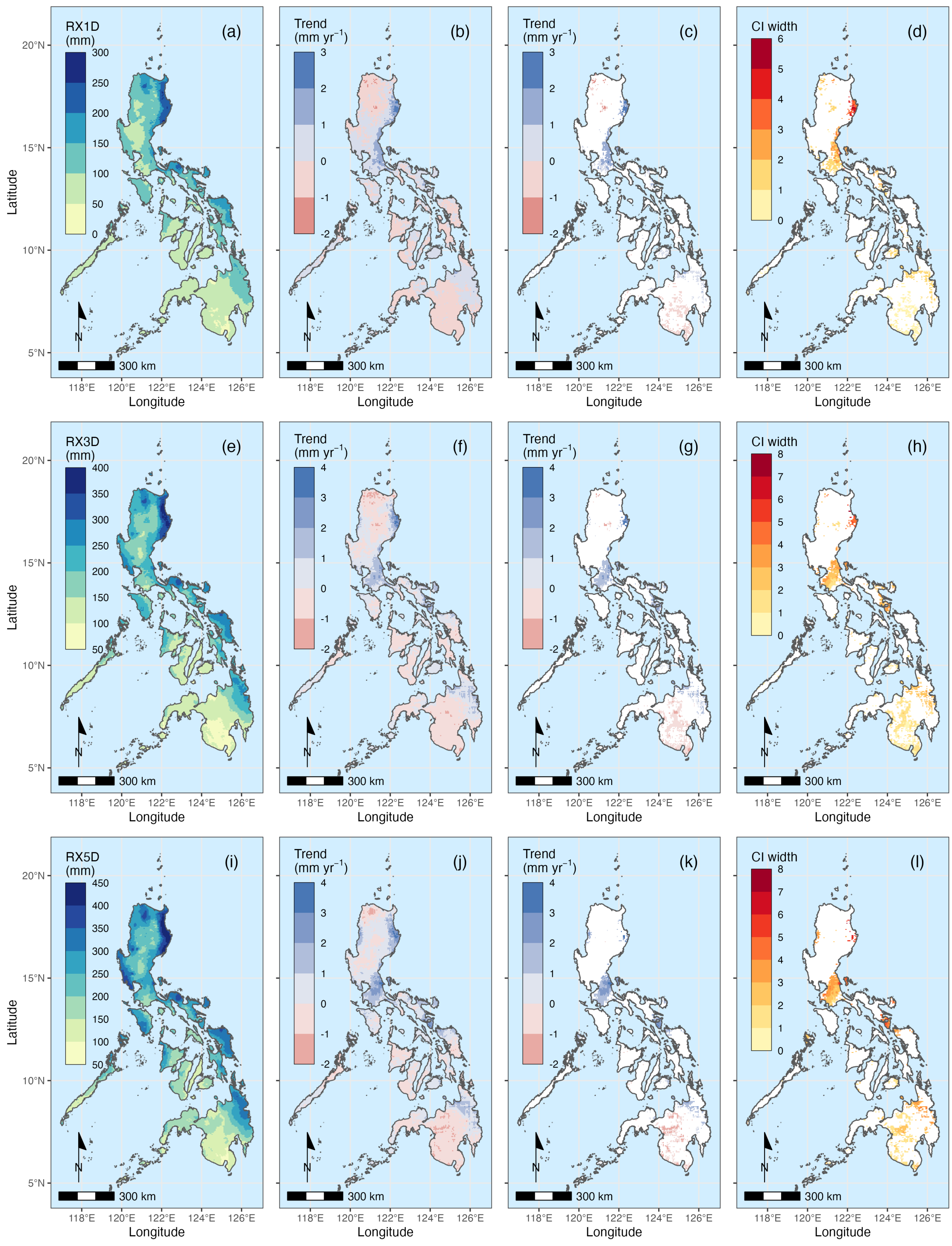

Figure 5. *Spatial distribution of mean annual maximum short-duration precipitation indices and their long-term trends across the Philippines derived from CHIRPS gridded rainfall data over the period 1981–2025. The upper row presents the maximum 1-day precipitation index (RX1day): panel (a) shows the mean annual RX1day (mm); panel (b) shows the Sen's slope estimate (mm yr^{-1}) for each grid cell, with blue tones denoting increasing trends and red tones denoting decreasing trends as indicated by the diverging color scale; panel (c) shows only those grid cells with statistically significant trends at α = 0.05 based on the Mann-Kendall trend test, with non-significant grid cells shown in white; and panel (d) shows the 95% confidence interval width (mm) of the Sen's slope estimate for each statistically*

significant grid cell, with darker red tones indicating wider confidence intervals (lower precision) and lighter yellow tones indicating narrower confidence intervals (higher precision), and non-significant grid cells shown in white. The middle row presents the corresponding maps for the maximum 3-day precipitation index (RX3day), following the same layout: panel (e) shows mean annual RX3day (mm); panel (f) shows the Sen's slope estimate; panel (g) shows statistically significant trends; and panel (h) shows the 95% confidence interval width (mm). The lower row presents the corresponding maps for the maximum 5-day precipitation index (RX5day): panel (i) shows mean annual RX5day (mm); panel (j) shows the Sen's slope estimate; panel (k) shows statistically significant trends; and panel (l) shows the 95% confidence interval width (mm). Note that the CI width color scales are consistent across RX3day and RX5day (0–7 mm) but slightly narrower for RX1day (0–6 mm), reflecting the progressively greater uncertainty in slope estimates for longer-accumulation maximum precipitation events. Non-significant grid cells are shown in white in panels (c), (d), (g), (h), (k), and (l).

3.1.4 Simple Daily Intensity Index (SDII)

Mean daily rainfall intensity on wet days (SDII) mirrors the established east-to-west gradient, with the highest values exceeding 35 mm day^{-1} concentrated along the eastern coastal zones of Luzon and the mountainous interior of northeastern Mindanao, and the lowest values falling below 10 mm day^{-1} across the western lowlands and leeward coastal areas (Fig. 6a). SDII trends are predominantly increasing across most of the archipelago (Fig. 6b).

Statistically significant increasing SDII trends covered 25.6% of land grid cells (Hamed-Rao-corrected; 31.9% raw), while significant decreasing trends were negligible (0.3%); this areal pattern did not reach field significance ($p = 0.058$) and is therefore suggestive of a weak intensification rather than a conclusive finding. Median Sen's slope and 95% CI values for the corrected significant-cell set are pending recomputation. The robust increase in heavy-rainfall-day frequency (R10, R20, R30), combined with an SDII signal that is directionally increasing but not field-significant, indicates that rainfall days are becoming more frequent with high confidence, while evidence for a corresponding change in per-event intensity remains inconclusive at the national scale; this is a more conservative conclusion than a straightforward frequency-versus-intensity dichotomy, though it retains practical relevance for flood frequency, soil erosion risk, and seasonal water availability.

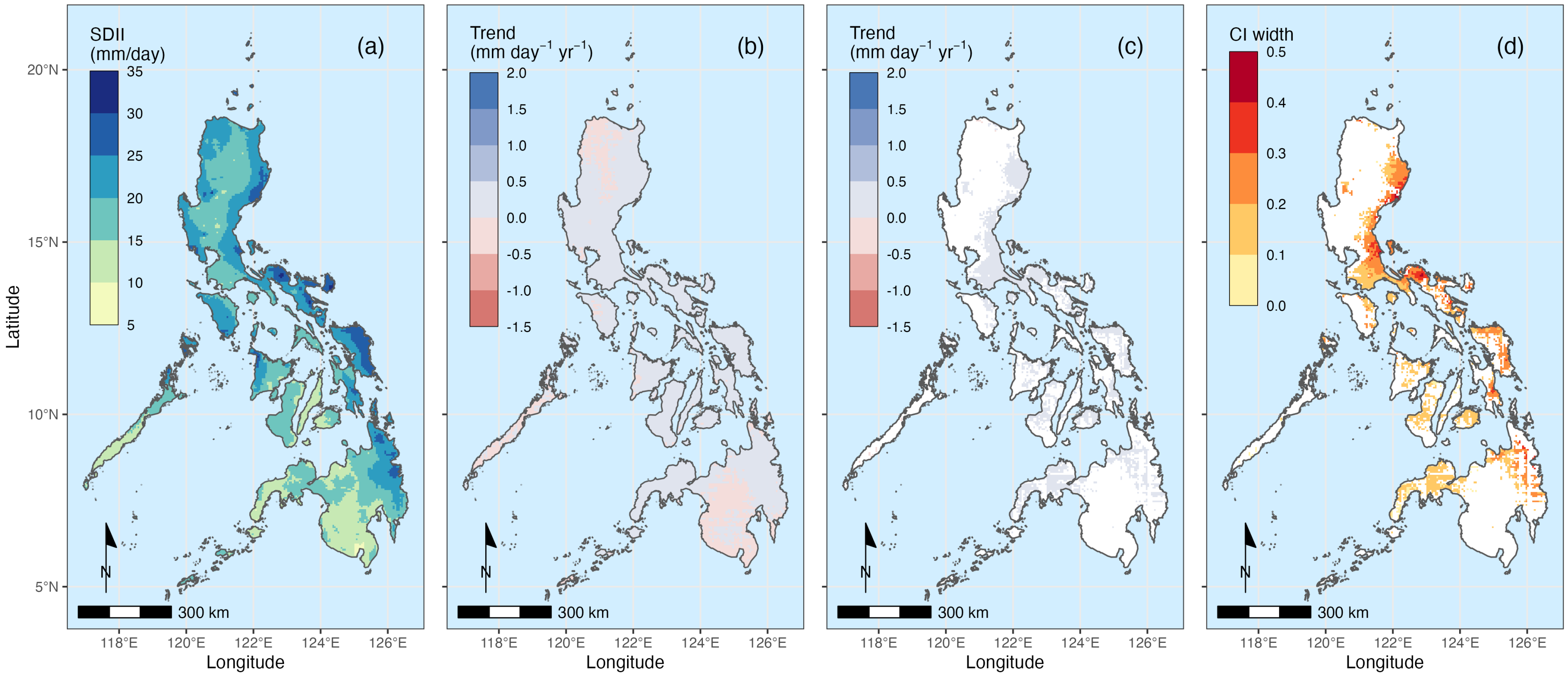

Figure 6. *Spatial distribution of mean annual Simple Daily Intensity Index (SDII) and its long-term trends across the Philippines derived from CHIRPS gridded rainfall data over the period 1981–2025. Panel (a) presents the mean annual SDII (mm day^{-1}), with higher values indicating greater mean rainfall intensity on wet days. Panel (b) presents the Sen's slope estimate (mm days^{-1} yr^{-1}) for each grid cell, with blue tones denoting increasing trends and red tones denoting decreasing trends as indicated by the diverging color scale. Panel (c) shows only those grid cells with statistically significant trends at α = 0.05 based on the Mann-Kendall trend test, with non-significant grid cells shown in white; color conventions follow panel (b). Panel (d) shows the 95% confidence interval width (mm days^{-1} yr^{-1}) of the Sen's slope estimate for each statistically significant grid cell, with darker red tones indicating wider confidence intervals (lower precision) and lighter yellow tones indicating narrower confidence intervals (higher precision); non-significant grid cells are shown in white. Note that the CI width scale for SDII (0–0.5 mm days^{-1} yr^{-1}) is substantially narrower than for the precipitation amount and short-duration indices, reflecting the high temporal consistency of the SDII trend signal across the archipelago.*

3.1.5 Consecutive Wet Days (CWD) and Consecutive Dry Days (CDD)

The markedly contrasting spatial distributions of CWD and CDD delineate the fundamental seasonality gradient of the Philippine climate system (Fig. 7a and e). Mean CWD values ranged from below 5 days in the western lowlands and leeward coastal areas to exceeding 50 days along the eastern coast of Luzon and the mountainous interior of northeastern Mindanao, while mean CDD values exhibited a spatially inverse pattern, with values exceeding 120 days concentrated across central and western Luzon, the western Visayas, and portions of western Mindanao, zones aligning with Type I climate, and near-zero values recorded along the eastern coast.

Statistically significant increasing CWD trends were spatially limited, covering 6.9% of land grid cells (Hamed-Rao-corrected; 5.0% raw) with a median slope of 0.1 days yr^{-1} (95% CI: 0.0–0.2 days yr^{-1}) (Fig. 7c; Table 2), though this pattern did not reach field significance ($p = 0.409$), indistinguishable from spatially correlated noise. Significant decreasing CDD trends covered 17.3% of land grid cells (Hamed-Rao-corrected; 8.8% raw) with a median slope of −0.2 days yr^{-1} (95% CI: −0.4 to −0.03 days yr^{-1}), predominantly concentrated in southern Mindanao (Fig. 7g; Table 2); this pattern also did not reach field significance ($p = 0.093$). The 95% CI width for significant CDD grid cells ranged up to 1.75 days yr^{-1} (Fig. 7h), nearly four times the maximum observed for CWD, reflecting the substantially greater interannual variability inherent in dry spell duration compared with wet spell persistence. The wide CI ranges relative to the median slope magnitudes for both indices indicate that while directional tendencies are detectable in specific sub-regions, trend estimates carry considerable uncertainty and should be interpreted with caution.

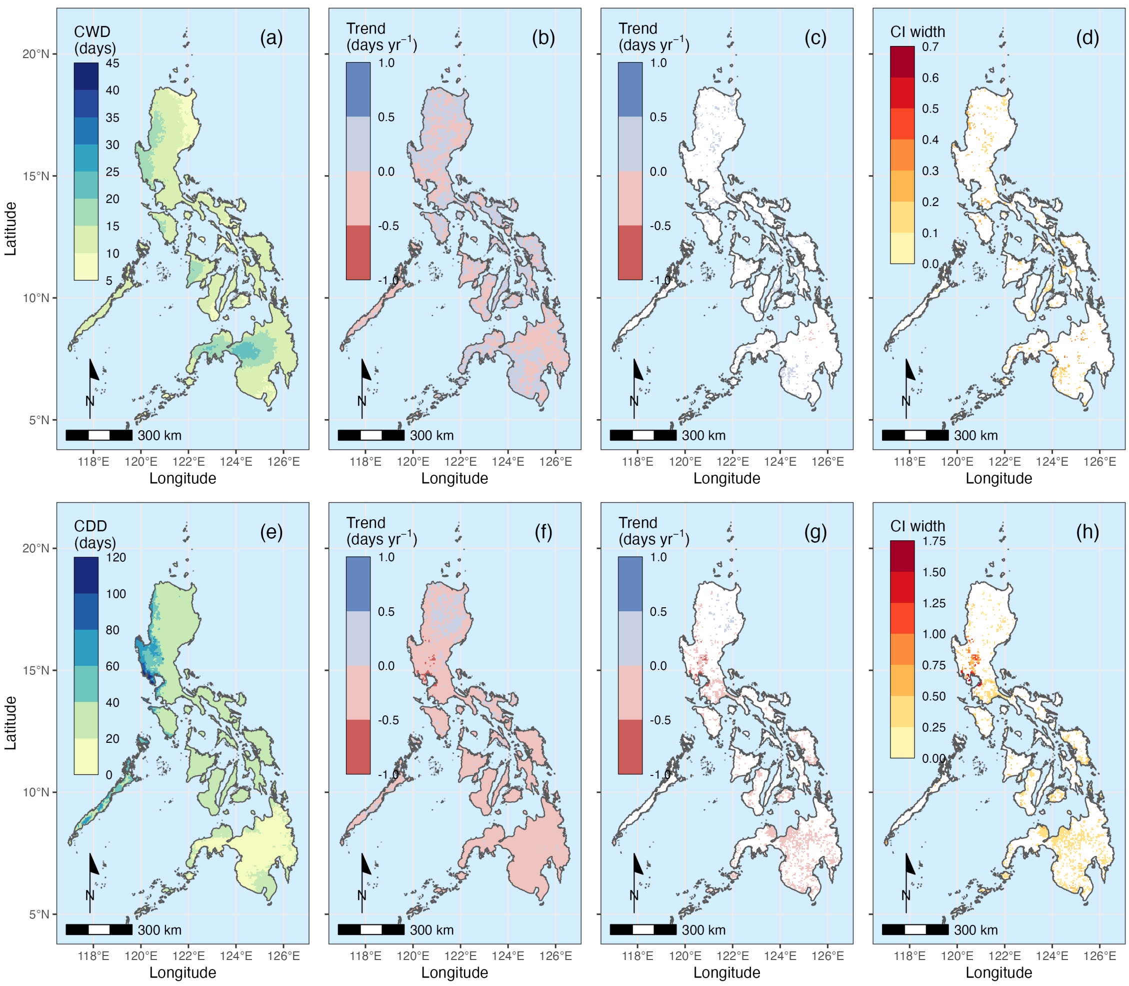

Figure 7. *Spatial distribution of mean annual consecutive wet days (CWD) and consecutive dry days (CDD) and their long-term trends across the Philippines derived from CHIRPS gridded rainfall data over the period 1981–2025. The upper row presents CWD: panel (a) shows the mean annual CWD (days); panel (b) shows the Sen's slope estimate (days yr^{-1}) for each grid cell, with blue tones denoting increasing trends and red tones denoting decreasing trends as indicated by the diverging color scale; panel (c) shows only those grid cells with statistically significant trends at $\alpha = 0.05$ based on the Mann-Kendall trend test, with non-significant grid cells shown in white; and panel (d) shows the 95% confidence interval width (days yr^{-1}) of the Sen's slope estimate for each statistically significant grid cell, with darker red tones indicating wider confidence intervals (lower precision) and lighter yellow tones indicating narrower confidence intervals (higher precision), and non-significant grid cells shown in white. The lower row presents the corresponding maps for CDD, following the same layout: panel (e) shows mean annual CDD (days); panel (f) shows the Sen's slope estimate (days yr^{-1}); panel (g) shows statistically significant trends, with blue tones denoting significant decreasing trends and red tones denoting significant increasing trends; and panel (h) shows the 95% confidence interval width (days yr^{-1}). Note that the CI width color scales differ substantially between CWD (0–0.45 days yr^{-1}) and CDD (0–1.75 days yr^{-1}), reflecting the greater interannual variability in dry spell duration relative to wet spell duration across the archipelago. Non-significant grid cells are shown in white in panels (c), (d), (g), and (h).*

3.1.6 Heavy Precipitation Days (R10, R20, and R30)

The heavy precipitation frequency indices exhibit the most spatially extensive and geographically coherent significant trend signal of all 12 EPIs examined. Mean R10 values ranged from below 20 days yr^{-1} in the driest western areas to exceeding 180 days yr^{-1} along the eastern coast of Luzon and eastern Mindanao; R20 and R30 exhibited a similar spatial structure at progressively lower magnitudes, with peak values approaching 120- and 80-days yr^{-1}, respectively (Fig. 8a, e, and i).

Statistically significant increasing trends for R10 were the most spatially extensive of any index in this study, covering 73.1% of land grid cells (Hamed-Rao-corrected; 63.0% raw) predominantly across Mindanao (34.4% of significant cells) and the Visayas (22.0%), with central and northern Luzon as secondary contributors, with a median Sen's slope of 0.6 days yr^{-1} (95% CI: 0.1–1.0 days yr^{-1}) (Fig. 8c; Table 2), field-significant at $p = 0.010$. Significant increasing trends for R20 covered 61.2% of land grid cells (Hamed-Rao-corrected; 56.2% raw) with a median slope of 0.4 days yr^{-1} (95% CI: 0.1–0.7 days yr^{-1}), broadly overlapping the R10 significant zone (Fig. 8g; Table 2), field-significant at $p = 0.007$. R30 showed significant increasing trends across 43.0% of land grid cells (Hamed-Rao-corrected; 40.4% raw) with a median slope of 0.3 days yr^{-1} (95% CI: 0.0–0.5 days yr^{-1}) (Fig. 8k; Table 2), field-significant at $p = 0.010$. All three frequency indices remain almost entirely one-directional, with negligible significant decreasing area (0.4% or less). Across all three indices, the maximum CI width narrows progressively from R10 to R30, from 1.8 days yr^{-1} to 1.0 days yr^{-1} (Fig. 8d, h, and l); this narrowing may reflect differing sensitivity to interannual variability across thresholds, though the scales and magnitudes also differ between indices, and this interpretation has not been statistically tested.

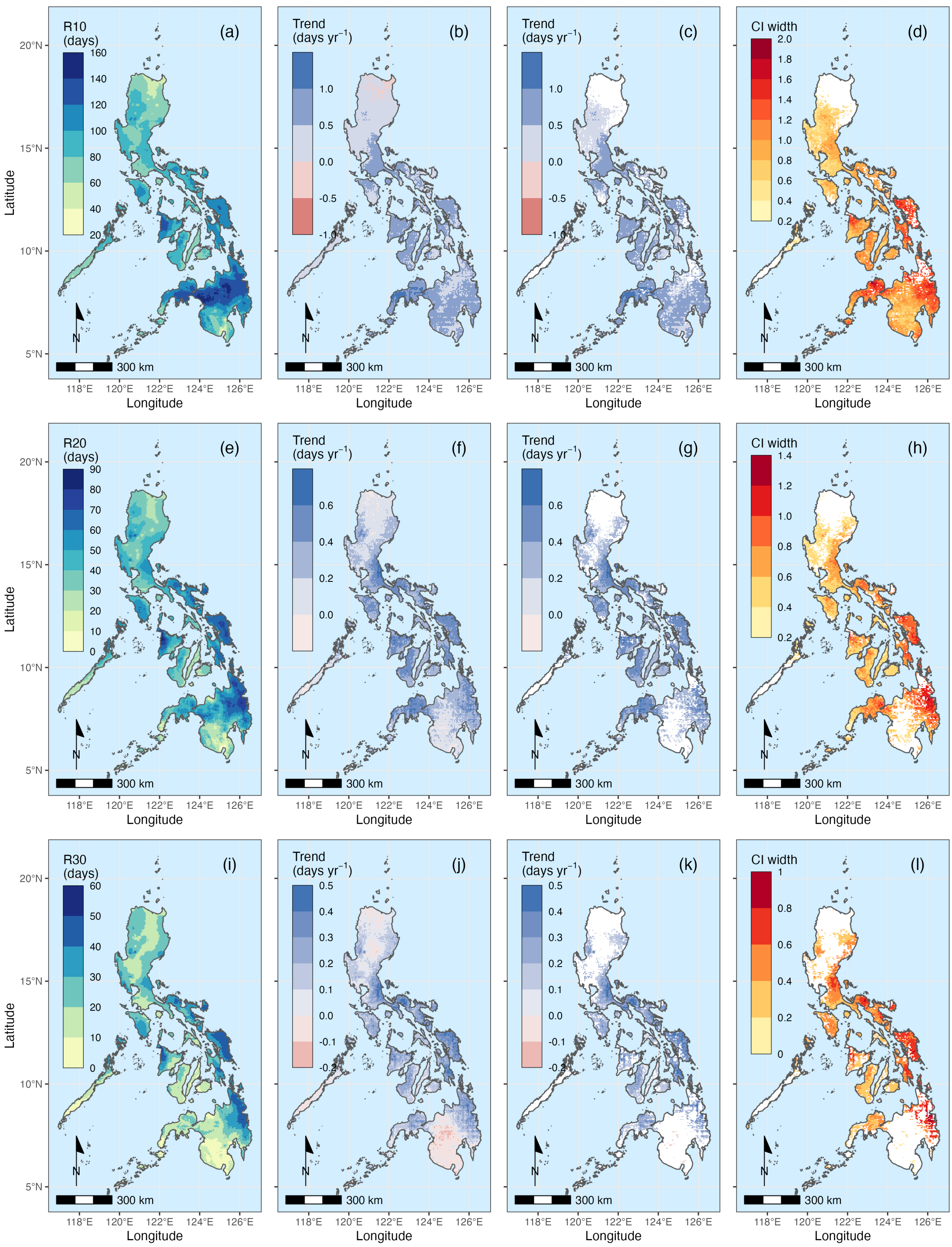

Figure 8. *Spatial distribution of mean annual heavy precipitation frequency indices and their long-term trends across the Philippines derived from CHIRPS gridded rainfall data over the period 1981–2025. The upper row presents the number of heavy precipitation days (R10): panel (a) shows the mean annual R10 (days); panel (b) shows the Sen's slope estimate (days yr^{-1}) for each grid cell, with blue tones denoting increasing trends and red tones denoting decreasing trends as indicated by the diverging color scale; panel (c) shows only those grid cells with statistically significant trends at α = 0.05 based on the Mann-Kendall trend test, with non-significant grid cells shown in white; and panel (d) shows the 95% confidence interval width (mm) of the Sen's slope estimate for each statistically significant grid cell, with*

darker red tones indicating wider confidence intervals (lower precision) and lighter yellow tones indicating narrower confidence intervals (higher precision), and non-significant grid cells shown in white. The middle row presents the corresponding maps for the number of very heavy precipitation days (R20), following the same layout: panel (e) shows mean annual R20 (days); panel (f) shows the Sen's slope estimate; panel (g) shows statistically significant trends; and panel (h) shows the 95% confidence interval width (mm). The lower row presents the corresponding maps for the number of extremely heavy precipitation days (R30): panel (i) shows mean annual R30 (days); panel (j) shows the Sen's slope estimate; panel (k) shows statistically significant trends; and panel (l) shows the 95% confidence interval width (mm). Note that the CI width color scales decrease progressively from R10 (0–1.8 mm) to R20 (0–1.2 mm) to R30 (0–1.0 mm); these scales are not directly comparable between rows. Non-significant grid cells are shown in white in panels (c), (d), (g), (h), (k), and (l).

3.2 EPI Trend Hotspots

LISA cluster classification was computed on the complete spatial field of Sen's slopes for each index (Section 3.1.0), rather than a subset pre-filtered to Mann-Kendall-significant cells. Across most indices, High-High hotspot clusters concentrate broadly on the typhoon-exposed eastern seaboard — eastern Mindanao, the eastern Visayas, and southern Luzon (Bicol) — while Low-Low coldspot clusters concentrate predominantly in northern Luzon and Palawan (Fig. 9); western Mindanao and the Zamboanga Peninsula depart from this general pattern for two indices, as described below. Spatial-outlier cells (High-Low, Low-High) account for less than 1% of land grid cells for every index, indicating that this clustering reflects genuine regional structure rather than noise.

For the precipitation amount indices, High-High clusters of PRCPTOT trends concentrate predominantly in eastern Mindanao, the eastern Visayas, and southern Luzon (Bicol) — rather than central Luzon specifically — within the broader eastern-seaboard pattern (Fig. 9, panel a). Low-Low clusters concentrate in northern Luzon and Palawan. R99p and R95p show broadly comparable High-High cluster locations to PRCPTOT (Fig. 9, panels b and c), consistent with the borderline field-significance of all three indices reported in Section 3.1.0.

For the short-duration maximum precipitation indices, RX1day, RX3day, and RX5day showed High-High clusters concentrated broadly along the eastern seaboard (Fig. 9, panels d–f); given that RX5day did not reach field significance (Section 3.1.0), the relative spatial extent of these clusters between RX3day and RX5day should not be read as confirming a lengthening of rainfall episodes, consistent with the more cautious framing adopted in Section 3.1.3. SDII showed a substantially broader High-High footprint than previously reported, spanning eastern central Luzon, eastern Mindanao, and eastern Bicol, consistent with the corrected, predominantly increasing SDII trend described in Section 3.1.4; a Low-Low cluster is also present, concentrated in western Mindanao and western/northern Luzon, and did not exist under the original, erroneous trend-direction classification (Fig. 9, panel g). CWD showed High-High clusters concentrated in western Mindanao, Palawan, and the eastern Visayas, and Low-Low clusters concentrated in eastern Mindanao, Palawan, and western Mindanao (Fig. 9, panel h). CDD showed High-High clusters (increasing dry-spell duration) concentrated in northern Luzon, and Low-Low clusters (decreasing dry-spell duration) concentrated in Palawan and western central Luzon; this differs from the geographic description in Section 3.1.5, where individually significant decreasing CDD cells are predominantly located in Mindanao (47.2% of significant cells) — the two descriptions capture different properties of the same field (spatially coherent clustering versus individual cell significance) and are not in conflict (Fig. 9, panel i).

The heavy precipitation frequency indices produced the most spatially extensive and statistically robust cluster patterns of all EPIs examined (Section 3.1.0). R10 exhibited High-High clusters concentrated predominantly in western Mindanao, the Zamboanga Peninsula, and eastern Mindanao, with the corresponding Low-Low coldspot located instead in northern Luzon (Fig. 9, panel j). R20 showed a broadly comparable pattern, with High-High clusters concentrated in eastern Mindanao and the Visayas and the coldspot again in northern Luzon (Fig. 9, panel k). R30 differs from R10 and R20 in this respect: its Low-Low coldspot is concentrated in western Mindanao — the same sub-region that is a High-High hotspot for R10 and R20 (Fig. 9, panel l). This reverses the practical implication for western Mindanao and the Zamboanga Peninsula relative to an assumption of uniform behaviour across the three frequency indices: rather than a coherent decline in heavy precipitation frequency, R10 and R20 indicate an escalating flood and erosion risk in this sub-region, while only R30 suggests a decline. High-High clusters for these indices spatially coincide with areas commonly reported as flood-prone in the Philippines (Abon et al., 2011; Rivera and Dela Vega, 2025), though this correspondence has not been independently validated against flood-hazard or exposure data.

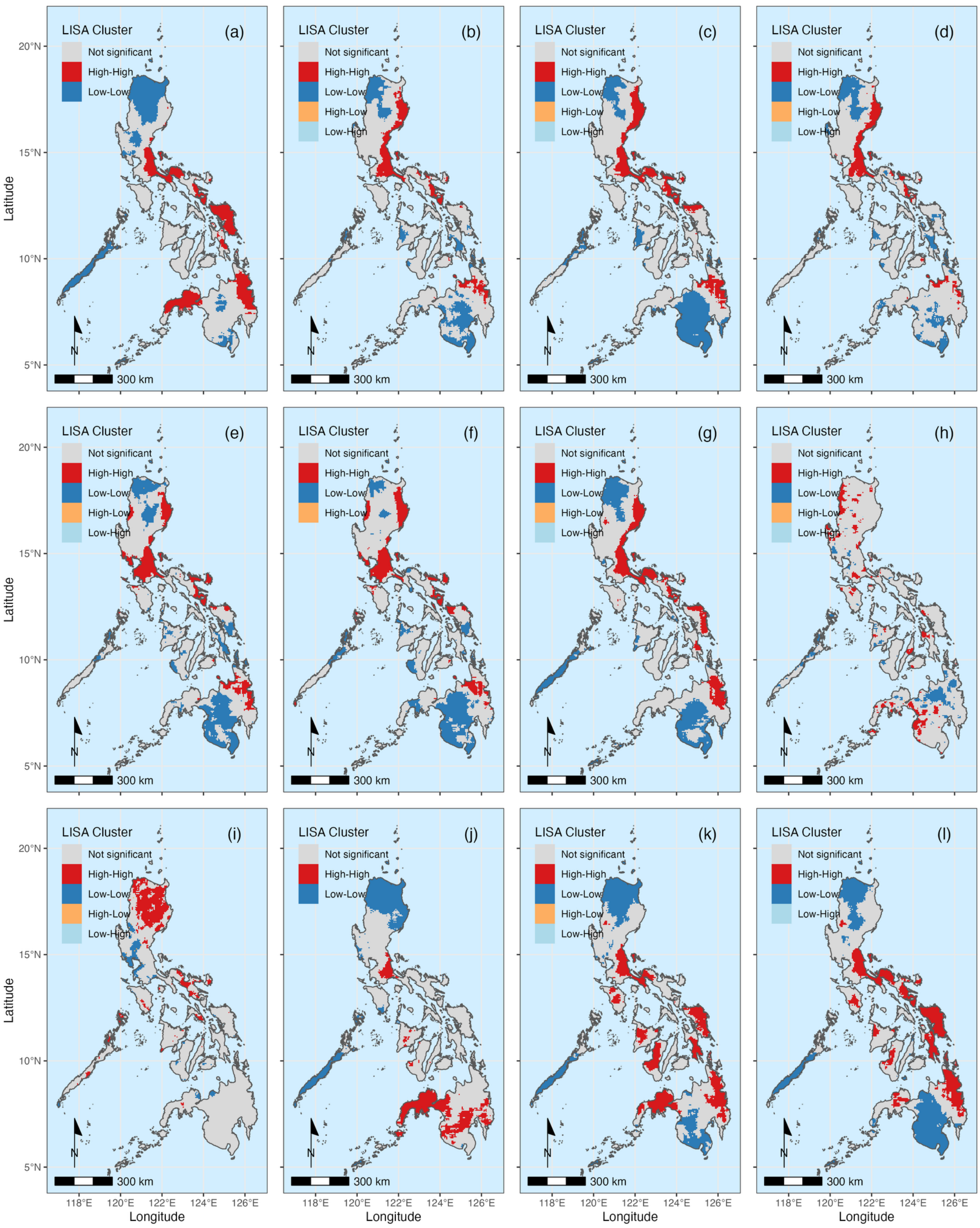

Figure 9. *Spatial distribution of Local Indicator of Spatial Association (LISA) cluster types for Sen's slope trend estimates of 12 extreme precipitation indices across the Philippines, 1981–2025. Each panel shows the LISA cluster classification for one EPI: (a) PRCPTOT, (b) R99p, (c) R95p, (d) RX1day, (e) RX3day, (f) RX5day, (g) SDII, (h) CWD, (i) CDD, (j) R10, (k) R20, and (l) R30. Cluster types are defined as follows: High-High indicates a grid cell with a high trend value surrounded by neighbors with similarly high trend values; Low-Low indicates a grid cell with a low trend value surrounded by neighbors with similarly low trend values; High-Low indicates a high trend value surrounded by low-trend neighbors; and Low-High indicates a low trend value surrounded by high-trend neighbors. Non-significant grid cells at α = 0.05 are shown in light grey. Cluster significance was assessed using 999 random permutations.*

4. DISCUSSION

The spatial pattern of EPI trends across the Philippines is not uniform but reflects the interplay of three dominant physical controls: orographic structuring of the rainfall climatology by the north-to-south mountain ranges of Luzon and Mindanao, differential typhoon track exposure between the eastern seaboard and the western lowlands, and ENSO-driven interannual modulation that amplifies drought conditions during warm phases and excess rainfall during cold phases (Lyon and Camargo, 2009; Moron et al., 2009). These controls collectively produce the east-to-west gradient evident in both the mean climatology and the spatial distribution of statistically significant trend signals, with increasing EPIs concentrated in the typhoon-exposed eastern seaboard and predominantly non-significant or declining signals across the leeward western and southern zones (Jose et al., 1996; Villafuerte et al., 2014).

The predominantly increasing PRCPTOT trends observed across Luzon and the Visayas are broadly consistent with global evidence for a general wetting tendency in recent decades (Dunn et al., 2022; Li et al., 2024). The median Sen's slope of 17.6 mm yr^{-1} (95% CI: 3.1–30.3 mm yr^{-1}) across significant grid cells is physically plausible under Clausius–Clapeyron scaling: rising sea surface temperatures in the western North Pacific increase available moisture along typhoon tracks, amplifying precipitation totals in the typhoon-exposed eastern seaboard zones where significant trends were most concentrated (Trenberth, 2011). These results differ from Cruz et al. (2013), who reported decreasing Southwest Monsoon rainfall across nine western Philippine stations from 1961 to 2010; this apparent discrepancy reflects complementary spatial coverage rather than contradiction, as the present study captures the full spatial extent of the archipelago including the eastern zones where increasing trends are strongest, while Cruz et al. (2013) sampled exclusively from the western seaboard where monsoon-season drying is the dominant signal.

Perhaps the most operationally significant finding of this study is the spatial separation between intensity-based and frequency-based precipitation indices, a pattern that constitutes the central and most policy-relevant result. Re-analysis found SDII trends to be predominantly increasing, not decreasing, across most of the archipelago, while R10, R20, and R30 showed even more strongly increasing trends across Luzon and the eastern Visayas. The significant SDII increase covered 25.6% of land grid cells (Hamed-Rao-corrected), though this pattern did not reach field significance ($p = 0.058$), while R10 showed significant increasing trends across 73.1% of land grid cells (field-significant, $p = 0.010$) with a median slope of 0.6 days yr^{-1} (95% CI: 0.1–1.0 days yr^{-1}). Rainfall days are therefore becoming more frequent with high statistical confidence, while evidence for a corresponding change in per-event intensity remains inconclusive; the convective-release mechanism proposed for a frequency-intensity contrast (Adam, 2023) should accordingly be read as a hypothesis for further investigation, since this study analysed precipitation indices only and did not examine convective activity, atmospheric moisture content, or storm type directly. The robust frequency increase nonetheless has direct agricultural consequences: increasing heavy rainfall frequency elevates the risk of waterlogging, runoff-driven soil erosion, and nitrate leaching without necessarily improving dry-season water availability for rainfed crops (Ren et al., 2025; Zhu et al., 2024).

For the short-duration maximum precipitation indices, significant trends were confined to the eastern coast of central Luzon, a sub-region sitting directly in the main western North Pacific typhoon track and encompassing some of the country's most flood-prone river basins. RX3day showed a significant decreasing trend (8.9% of land grid cells, Hamed-Rao-corrected; field-significant, $p = 0.044$; median slope: −0.5 mm yr^{-1}; 95% CI: −1.0 to −0.02 mm yr^{-1}) while RX5day showed a significant increasing trend (8.6%; not field-significant, $p = 0.115$; median slope: 1.4 mm yr^{-1}; 95% CI: 0.1–2.7 mm yr^{-1}). Because RX5day does not reach field significance, this contrast is better characterised as a pattern warranting further, event-based investigation than as evidence of a systematic lengthening of rainfall episodes; any connection to slow-moving or stalling typhoon behaviour under warming conditions should be presented as a hypothesis drawn from the external literature, since tropical cyclone tracks, translation speed, and duration were not analysed in this study. Much of Mindanao, Palawan, and the Zamboanga Peninsula showed no statistically significant directional change in any short-duration index, demonstrating that national-level averages would obscure critical sub-regional contrasts.

The CWD and CDD results point to important shifts in the spell-duration structure of Philippine rainfall, though the spatial extent of statistically significant trends remains limited. Significant CWD increasing trends covered 6.9% of land grid cells (Hamed-Rao-corrected; median slope: 0.1 days yr^{-1}; 95% CI: 0.0–0.2 days yr^{-1}), while significant decreasing CDD trends covered 17.3% (Hamed-Rao-corrected, concentrated in southern Mindanao; median slope: −0.2 days yr^{-1}; 95% CI: −0.4 to −0.03 days yr^{-1}). Neither pattern reached field significance (CWD: $p = 0.409$; CDD: $p = 0.093$), with CWD's spatial pattern indistinguishable from what spatial autocorrelation alone would produce; the wet-gets-wetter, dry-gets-drier interpretation

(Trenberth, 2011) should therefore be read as a hypothesis motivated by the robust frequency-index findings rather than as independently supported by the CWD/CDD trends themselves. These opposing tendencies have direct implications for water resource management, particularly in Type I and Type III climate zones of western and inland Luzon where an already-pronounced dry season limits agricultural and municipal water availability, necessitating investment in dry-season water storage and demand management strategies.

LISA cluster classification was computed on the complete spatial field of Sen's slopes, rather than a subset pre-filtered to already-significant cells, since filtering first would condition the neighbourhood structure on a prior significance test and risk exaggerating apparent clustering. Substantial coherent clustering was found, with spatial-outlier cells (High-Low, Low-High) accounting for less than 1% of land grid cells across every index, indicating that the observed clustering reflects genuine regional structure rather than noise. High-High clusters for PRCPTOT and most other indices concentrate in eastern Mindanao, the eastern Visayas, and the Bicol region, within a broader eastern-seaboard pattern. Western Mindanao and the Zamboanga Peninsula are a High-High (increasing-frequency) hotspot for R10 and R20 rather than a Low-Low coldspot; only R30 shows a coldspot pattern in this sub-region, while the R10/R20 coldspot is instead located in northern Luzon. This carries a different practical implication for western Mindanao and the Zamboanga Peninsula than a uniform frequency decline would: rather than a coherent decline in heavy precipitation frequency compounding dry-season water stress, the evidence points to an escalating flood and erosion risk for two of the three frequency indices. The apparent correspondence between High-High clusters and the country's most flood-prone zones (Abon et al., 2011; Rivera and Dela Vega, 2025) has not been independently validated against flood-hazard or exposure data. These results should inform prioritisation of climate adaptation investment, early warning infrastructure, and disaster risk reduction planning across the exposure-sensitive sub-regions identified above.

5. Limitations

The primary methodological constraint of this study is its reliance on CHIRPS gridded precipitation data in the absence of a spatially comprehensive ground-based gauge network. Although CHIRPS has been validated for the Philippines and demonstrated adequate performance in capturing seasonal rainfall patterns (Alejo and Alejandro, 2021; Peralta et al., 2020), the dataset tends to underestimate rainfall from May to October and its performance varies systematically across the four Philippine climate types. In areas with sparse gauge coverage, including mountainous interiors and open ocean-facing coastal zones, trend estimates may be less reliable. Establishing a denser national gauge network and integrating those observations into future CHIRPS validation exercises would directly improve the spatial reliability of national-scale EPI trend assessments.

A second limitation concerns the potential confounding of long-term anthropogenic trends by ENSO-driven interannual variability. The Mann-Kendall trend test assumes temporal independence of the data series, yet Philippine rainfall is strongly modulated by ENSO, which introduces low-frequency variability that can inflate or suppress the apparent significance of long-term trends. This has now been partially addressed: a Hamed-Rao (1998) autocorrelation correction and a spatial field-significance test have been applied to all 12 indices (Section 3.1.0), and the results reported throughout Sections 3 and 4 reflect this correction. Incorporating ENSO phase as an explicit covariate remains a valuable direction for future work, as the correction applied here addresses temporal autocorrelation generally rather than attributing it specifically to ENSO.

A related limitation concerns the percentile thresholds used for R95p and R99p, which were calculated from the full 1981–2025 record rather than an independent, non-overlapping reference period, since CHIRPS coverage begins in 1981 and no earlier independent baseline was available. Calculating a percentile threshold from the same record used to detect a trend can partially absorb that trend into the threshold itself, which would tend to understate rather than overstate the true R95p/R99p signal. This is consistent with the R95p and R99p trends reported here being the most conservative, least field-significant results among the amount- and intensity-based indices, and should be kept in mind when comparing these results with studies using an independent base period.

Third, the 0.05° (approximately 5 km) spatial resolution of CHIRPS is insufficient to resolve sub-kilometre orographic precipitation gradients in complex terrain such as the Cordillera Central of northern Luzon and the mountainous spine of Mindanao. Orographic enhancement at scales below 5 km may be smoothed in the CHIRPS grid, potentially leading to underestimation of trend magnitudes in topographically complex areas. High-resolution dynamical downscaling or statistical bias correction against dense gauge networks in these regions would improve the spatial precision of trend estimates in areas where orographic effects are most pronounced.

Fourth, the 45-year study period, while adequate for Mann-Kendall trend detection under standard power requirements, may be insufficient to fully separate anthropogenically forced signals from multi-decadal natural variability in indices such as CDD and CWD that exhibit high interannual variance. Extending the analysis using dynamically downscaled historical simulations or longer reconstructed precipitation records would provide a more robust temporal baseline against which the observed trends can be contextualised.

Finally, this study characterised trends using annual EPI values only. Seasonal decomposition of trends, for example, isolating the typhoon season (June–November) from the northeast monsoon season (December–February), would provide considerably finer insight into which periods of the year are driving the observed annual signals, and would be more directly actionable for sectoral planning across agriculture, water resources, and disaster risk management. This is identified as a priority direction for follow-on work.

6. Conclusion

Extreme precipitation change across the Philippines is spatially selective, physically structured, and index-family-specific, concentrated on the typhoon-exposed eastern seaboard rather than distributed uniformly across the archipelago. By applying Mann-Kendall trend testing, Theil-Sen slope estimation with 95% confidence intervals, and LISA spatial autocorrelation to 45 years of CHIRPS daily precipitation data (1981–2025), this study provides the first spatially comprehensive, multi-index assessment of EPI trends at national scale, directly addressing the limited spatial coverage and narrow index sets that characterised earlier Philippine precipitation trend studies.

Total annual precipitation (PRCPTOT) shows the most statistically robust amount-based signal, with a field-significant increasing trend covering 71.9% of land grid cells ($p = 0.004$), concentrated predominantly across Mindanao and the Visayas rather than central Luzon specifically. R99p and R95p show a similar increasing pattern but do not reach field significance, and should be regarded as suggestive rather than conclusively established. Much of Mindanao, Palawan, and the Zamboanga Peninsula showed no significant directional change in any amount or intensity index over the study period.

The central finding of this study is that rainfall days are becoming more frequent across much of the Philippines with high statistical confidence, while evidence for a corresponding change in the intensity of individual rainfall events remains inconclusive. Heavy precipitation frequency (R10, R20, R30) shows the most spatially extensive and statistically robust signal of any index examined, covering up to 73.1% of land grid cells and field-significant for all three indices ($p \leq 0.010$). SDII shows a significant increasing trend across 25.6% of land grid cells, though this pattern does not reach field significance. This distinction carries direct consequences for flood risk, agricultural water management, and soil erosion planning.

The contrasting short-duration trends in RX3day (decreasing, field-significant) and RX5day (increasing, not field-significant) are suggestive of, but do not on their own demonstrate, a lengthening of sustained rainfall episodes, since the RX5day pattern cannot be distinguished from spatially correlated noise. Any connection to tropical cyclone stalling behaviour under warming conditions should be treated as a hypothesis for further, event-based investigation rather than an established finding.

LISA confirms substantial coherent spatial clustering for most indices, with negligible spatial-outlier area, indicating genuine regional structure rather than noise. Western Mindanao and the Zamboanga Peninsula are a High-High hotspot of increasing frequency for R10 and R20 rather than a coldspot; only R30 shows a coldspot pattern in this sub-region, while the R10/R20 coldspot is instead located in northern Luzon. This carries a different practical implication than a uniform frequency decline would: an escalating flood and erosion risk for two of the three frequency indices in western Mindanao and the Zamboanga Peninsula, alongside a water-stress-relevant decline concentrated in northern Luzon.

These findings support the development of location-specific, index-disaggregated precipitation monitoring and early warning systems across the eastern seaboard of Mindanao, the Visayas, and southern Luzon (Bicol), including western Mindanao and the Zamboanga Peninsula for the R10 and R20 frequency indices specifically, where the robust intensification of rainfall totals and heavy precipitation frequency represents an escalating flood and erosion risk. Agricultural water planning in northern Luzon, where the R10/R20 coldspot is located, should account for the potential decline in heavy precipitation frequency suggested here. These applications are presented as priorities for further validation rather than as immediate operational recommendations, given the statistical qualifications described above, including the borderline field-significance of several indices, so as not to overstate what a trend-only analysis using CHIRPS can support for operational decisions.

Data availability statement

CHIRPS data set can be downloaded at the Climate Hazards Center, University of Santa Barbara website (https://data.chc.ucsb.edu/)

Conflict of interest

The authors declare no competing interests.

Contributor Role Taxonomy (CRediT)

Conceptualization: ARS
Methodology: ARS
Validation: ARS
Formal analysis and investigation: ARS
Writing - original draft preparation: ARS, ALN, DSL
Writing - review and editing: ARS, ALN, DSL
Visualization: ARS

ORCID

Arnold R. Salvacion, ORCID: 0000-0001-8868-2226
Allen L. Nazareno, ORCID: 0000-0002-8969-6774
Destiny S. Lutero, ORCID: 0000-0001-8616-3852

References

Abdullah, A.Y.Md., Bhuian, Md.H., Kiselev, G., Dewan, A., Hassan, Q.K., Rafiuddin, M., 2022. Extreme temperature and rainfall events in Bangladesh: A comparison between coastal and inland areas. International Journal of Climatology 42, 3253–3273. https://doi.org/10.1002/joc.6911

Abon, C.C., David, C.P.C., Pellejera, N.E.B., 2011. Reconstructing the tropical storm ketsana flood event in marikina river, philippines. Hydrology and Earth System Sciences 15, 1283–1289. https://doi.org/10.5194/hess-15-1283-2011

Ajjur, S.B., Al-Ghamdi, S.G., 2021. Evapotranspiration and water availability response to climate change in the Middle East and North Africa. Climatic Change 166, 28. https://doi.org/10.1007/s10584-021-03122-z

Alejo, L.A., Alejandro, A.S., 2021. Validating CHIRPS ability to estimate rainfall amount and detect rainfall occurrences in the Philippines. Theoretical and Applied Climatology 145, 967–977. https://doi.org/10.1007/s00704-021-03685-y

Andhikaputra, G., Sapkota, A., Lin, Y.-K., Chan, T.-C., Gao, C., Deng, L.-W., Wang, Y.-C., 2023. The impact of temperature and precipitation on all-infectious-, bacterial-, and viral-diarrheal disease in taiwan. Science of The Total Environment 862, 160850. https://doi.org/10.1016/j.scitotenv.2022.160850

Anselin, L., 1995. Local Indicators of Spatial AssociationLISA. Geographical Analysis 27, 93–115. https://doi.org/10.1111/j.1538-4632.1995.tb00338.x

Boquet, Y., 2017. 7107 Islands, in: Boquet, Y. (Ed.),. Springer International Publishing, Cham, pp. 11–36. https://doi.org/10.1007/978-3-319-51926-5_2

Bronaugh, D., Schoeneberg, A., 2023. Zyp: Zhang + yue-pilon trends package. https://doi.org/10.32614/CRAN.package.zyp

Cinco, T.A., Guzman, R.G. de, Hilario, F.D., Wilson, D.M., 2014. Long-term trends and extremes in observed daily precipitation and near surface air temperature in the philippines for the period 19512010. Atmospheric Research 145-146, 12–26. https://doi.org/10.1016/j.atmosres.2014.03.025

Cruz, F.T., Narisma, G.T., Villafuerte, M.Q., Cheng Chua, K.U., Olaguera, L.M., 2013. A climatological analysis of the southwest monsoon rainfall in the philippines. Atmospheric Research 122, 609–616. https://doi.org/10.1016/j.atmosres.2012.06.010

Delforge, D., Wathelet, V., Below, R., Sofia, C.L., Tonnelier, M., Loenhout, J.A.F. van, Speybroeck, N., 2025. EM-DAT: The emergency events database. International Journal of Disaster Risk Reduction 124, 105509. https://doi.org/10.1016/j.ijdrr.2025.105509

Deng, H., Li, G., Pan, X., Wang, Q., Xiao, Z., 2026. Quantifying the impact of extreme climatic compound events and adaptation strategies on seed maize yield: Insights from a six-year field experiment in the hexi corridor oasis, china. European Journal of Agronomy 172, 127864. https://doi.org/10.1016/j.eja.2025.127864

Du, H., Tan, M.L., Zhang, F., Chun, K.P., Li, L., Kabir, M.H., 2024. Evaluating the effectiveness of CHIRPS data for hydroclimatic studies. Theoretical and Applied Climatology 155, 1519–1539. https://doi.org/10.1007/s00704-023-04721-9

Dunn, R.J.H., Donat, M.G., Alexander, L.V., 2022. Comparing extremes indices in recent observational and reanalysis products. Frontiers in Climate 4. https://doi.org/10.3389/fclim.2022.989505

Evans, J.S., Murphy, M.A., 2025. spatialEco.

Fattahi, E., Kamali, S., Oskouei, E.A., Habibi, M., 2025. Investigating the Spatiotemporal Variation in Extreme Precipitation Indices in Iran from 1990 to 2020. Water 17. https://doi.org/10.3390/w17081227

Funk, C., Peterson, P., Landsfeld, M., Pedreros, D., Verdin, J., Shukla, S., Husak, G., Rowland, J., Harrison, L., Hoell, A., Michaelsen, J., 2015. The climate hazards infrared precipitation with stationsa new environmental record for monitoring extremes. Scientific Data 2, 150066. https://doi.org/10.1038/sdata.2015.66

Gan, R., Li, D., Chen, C., Yang, F., Ma, X., 2022. Impacts of climate change on extreme precipitation in the upstream of Chushandian reservoir, China. Hydrology Research 53, 504–518. https://doi.org/10.2166/nh.2022.135

Hamed, K.H., 2008. Trend detection in hydrologic data: The mannkendall trend test under the scaling hypothesis. Journal of Hydrology 349, 350–363. https://doi.org/10.1016/j.jhydrol.2007.11.009

Ibarra, D.E., David, C.P.C., Tolentino, P.L.M., 2021. Technical note: Evaluation and bias correction of an observation-based global runoff dataset using streamflow observations from small tropical catchments in the philippines. Hydrology and Earth System Sciences 25, 2805–2820. https://doi.org/10.5194/hess-25-2805-2021

Karimzadeh, S., Ahmadi, A., Baldocchi, D., Fisher, J.B., 2025. Climate change has increased global evaporative demand except in South Asia. Communications Earth & Environment 6, 1009. https://doi.org/10.1038/s43247-025-02959-x

Li, S., Chen, Y., Wei, W., Fang, G., Duan, W., 2024. The increase in extreme precipitation and its proportion over global land. Journal of Hydrology 628, 130456. https://doi.org/10.1016/j.jhydrol.2023.130456

Li, Y., Bai, J., You, Z., Hou, J., Li, W., 2021. Future changes in the intensity and frequency of precipitation extremes over China in a warmer world: Insight from a large ensemble. PLOS ONE 16, e0252133. https://doi.org/10.1371/journal.pone.0252133

Lima, M.I.P. de, Santo, F.E., Ramos, A.M., Trigo, R.M., 2015. Trends and correlations in annual extreme precipitation indices for mainland Portugal, 19412007. Theoretical and Applied Climatology 119, 55–75. https://doi.org/10.1007/s00704-013-1079-6

Liu, J., Yu, W., Pan, R., He, Y., Wu, Y., Yan, S., Yi, W., Li, X., Song, R., Yuan, J., Liu, L., Wei, N., Jin, X., Li, Y., Liang, Y., Sun, X., Mei, L., Song, J., Cheng, J., Su, H., 2022. Association between sequential extreme precipitation-heatwaves events and hospitalizations for schizophrenia: The damage amplification effects of sequential extremes. Environmental Research 214, 114143. https://doi.org/10.1016/j.envres.2022.114143

Massicotte, P., South, A., 2026. Rnaturalearth: World map data from natural earth. https://doi.org/10.32614/CRAN.package.rnaturalearth

Mullens, E.D., Shafer, M., Hocker, J., 2013. Trends in heavy precipitation in the southern USA. Weather 68, 311–316. https://doi.org/10.1002/wea.2113

Nguyen, H.M., Ouillon, S., Vu, V.D., 2022. Sea Level Variation and Trend Analysis by Comparing MannKendall Test and Innovative Trend Analysis in Front of the Red River Delta, Vietnam (19612020). Water 14. https://doi.org/10.3390/w14111709

Ogolo, E.O., Matthew, O.J., 2022. Spatial and temporal analysis of observed trends in extreme precipitation events in different climatic zones of Nigeria. Theoretical and Applied Climatology 148, 1335–1351. https://doi.org/10.1007/s00704-022-04006-7

Olaguera, L.M.P., Cruz, F.A.T., Dado, J.M.B., Villarin, J.R.T., 2022. Complexities of Extreme Rainfall in the Philippines, in: Unnikrishnan, A.S., Tangang, F., Durrheim, R.J. (Eds.),. Springer Nature, Singapore, pp. 129–146. https://doi.org/10.1007/978-981-19-2511-5_5

Peralta, J.C.A.C., Narisma, G.T.T., Cruz, F.A.T., 2020. Validation of High-Resolution Gridded Rainfall Datasets for Climate Applications in the Philippines. Journal of Hydrometeorology 21, 1571–1587. https://doi.org/10.1175/JHM-D-19-0276.1

R Core Team, 2025. R: A language and environment for statistical computing. R Foundation for Statistical Computing, Vienna, Austria.

Rana, A., Foster, K., Bosshard, T., Olsson, J., Bengtsson, L., 2014. Impact of climate change on rainfall over mumbai using distribution-based scaling of global climate model projections. Journal of Hydrology: Regional Studies 1, 107–128. https://doi.org/10.1016/j.ejrh.2014.06.005

Ren, Z., Zhao, H., Mu, X., Shi, K., Jin, X., 2025. Characteristics of extreme precipitation and its effects on soil and water retention in sichuan, china under multiple climate change elements. Ecological Indicators 176, 113702. https://doi.org/10.1016/j.ecolind.2025.113702

Rivera, A.T., Dela Vega, J.B.G., 2025. From vulnerability to resilience: Addressing the causes, impacts, and solutions for recurrent flash floods in the philippines. Tropical Cyclone Research and Review 14, 301–310. https://doi.org/10.1016/j.tcrr.2025.08.005

Rodríguez-González, M.P., Cerezo-Mota, R., 2025. Trend Analysis of Extreme Precipitation Indices and Climate Oscillations Over the Yucatan Peninsula for the Period 19802010. International Journal of Climatology 45, e8885. https://doi.org/10.1002/joc.8885

Rojpratak, S., Supharatid, S., 2022. Regional extreme precipitation index: Evaluations and projections from the multi-model ensemble CMIP5 over thailand. Weather and Climate Extremes 37, 100475. https://doi.org/10.1016/j.wace.2022.100475

Saddique, N., Khaliq, A., Bernhofer, C., 2020. Trends in temperature and precipitation extremes in historical (19611990) and projected (20612090) periods in a data scarce mountain basin, northern Pakistan. Stochastic Environmental Research and Risk Assessment 34, 1441–1455. https://doi.org/10.1007/s00477-020-01829-6

Salvacion, A.R., Magcale-Macandog, D.B., Cruz, P.C.Sta., Saludes, R.B., Pangga, I.B., Cumagun, C.J.R., 2018. Evaluation and spatial downscaling of CRU TS precipitation data in the Philippines. Modeling Earth Systems and Environment 4, 891–898. https://doi.org/10.1007/s40808-018-0477-2

Santos, C.A.C. dos, Neale, C.M.U., Mekonnen, M.M., Gonçalves, I.Z., Oliveira, G. de, Ruiz-Alvarez, O., Safa, B., Rowe, C.M., 2022. Trends of extreme air temperature and precipitation and their impact on corn and soybean yields in Nebraska, USA. Theoretical and Applied Climatology 147, 1379–1399. https://doi.org/10.1007/s00704-021-03903-7

Sousa, K. de, Etten, J. van, Neby, M., Solberg, S.Ø., 2023. Climate variability indices for ecological and crop models in R: the climatrends package. Journal of Open Source Software 8, 4405. https://doi.org/10.21105/joss.04405

Tabari, H., 2020. Climate change impact on flood and extreme precipitation increases with water availability. Scientific Reports 10, 13768. https://doi.org/10.1038/s41598-020-70816-2

Tang, C., Liu, X., He, Y., Gao, J., Xu, Z., Duan, J., Yi, W., Wei, Q., Pan, R., Song, S., Su, H., 2020. Association between extreme precipitation and ischemic stroke in hefei, china: Hospitalization risk and disease burden. Science of The Total Environment 732, 139272. https://doi.org/10.1016/j.scitotenv.2020.139272

Techamahasaranont, J., Shrestha, S., Babel, M.S., Shrestha, R.P., Jourdain, D., 2017. Spatial and temporal variation in the trends of hydrological response of forested watersheds in Thailand. Environmental Earth Sciences 76, 430. https://doi.org/10.1007/s12665-017-6764-9

Theil, H., 1992. A Rank-Invariant Method of Linear and Polynomial Regression Analysis, in: Raj, B., Koerts, J. (Eds.),. Springer Netherlands, Dordrecht, pp. 345–381. https://doi.org/10.1007/978-94-011-2546-8_20

Tolentino, P.L.M., Poortinga, A., Kanamaru, H., Keesstra, S., Maroulis, J., David, C.P.C., Ritsema, C.J., 2016. Projected Impact of Climate Change on Hydrological Regimes in the Philippines. PLOS ONE 11, e0163941. https://doi.org/10.1371/journal.pone.0163941

Trenberth, K.E., 2011. Changes in precipitation with climate change. Climate Research 47, 123–138. https://doi.org/10.3354/cr00953

Vahmani, P., Jones, A.D., Li, D., 2022. Will Anthropogenic Warming Increase Evapotranspiration? Examining Irrigation Water Demand Implications of Climate Change in California. Earth's Future 10, e2021EF002221. https://doi.org/10.1029/2021EF002221

Villafuerte, M.Q., Matsumoto, J., Akasaka, I., Takahashi, H.G., Kubota, H., Cinco, T.A., 2014. Long-term trends and variability of rainfall extremes in the philippines. Atmospheric Research 137, 1–13. https://doi.org/10.1016/j.atmosres.2013.09.021

Wang, L., Wang, J., He, F., Wang, Q., Zhao, Y., Lu, P., Huang, Y., Cui, H., Deng, H., Jia, X., 2023. Spatialtemporal variation of extreme precipitation in the YellowHuaiHaiYangtze Basin of China. Scientific Reports 13, 9312. https://doi.org/10.1038/s41598-023-36470-0

WCRP, 2025. Expert team on climate change detection and indices (ETCCDI).

Yumul, G.P., Servando, N.T., Suerte, L.O., Magarzo, M.Y., Juguan, L.V.V., Dimalanta, C.B., 2012. Tropical cyclonesouthwest monsoon interaction and the 2008 floods and landslides in Panay island, central Philippines: meteorological and geological factors. Natural Hazards 62, 827–840. https://doi.org/10.1007/s11069-012-0109-5

Zhang, X., Alexander, L., Hegerl, G.C., Jones, P., Klein Tank, A., Peterson, T.C., Trewin, B., Zwiers, F.W., 2011. Indices for monitoring changes in extremes based on daily temperature and precipitation data. Wiley Interdisciplinary Reviews: Climate Change 2, 851–870. https://doi.org/10.1002/wcc.147

Zhu, X., Miao, P., Zhu, H., Li, W., Liang, X., Wang, L., Chen, Z., Zhou, J., 2024. Extreme precipitation accelerates nitrate leaching in the intensive agricultural region with thick unsaturated zones. Science of The Total Environment 918, 170789. https://doi.org/10.1016/j.scitotenv.2024.170789